MICROCOPY RESOLUTION TEST CHART

NATIONAL BUREAU OF STANDARDS-1963-A

AFGL -TR-83-0162

ANALYSIS AND INVESTIGATION OF THE
EFFECTS OF ATMOSPHERIC GRAVITY
WAVES ON INFRARED EMISSIONS

Tai-Fu-Tuan

University of Cincinnati
Physics Department
Cincinnati, Ohio 45221

Final Report
September 1, 1980 - August 31, 1983

May 30, 1983

DTIC
ELECTE
NOV 26 1984
A

AIR FORCE GEOPHYSICS LABORATORY
AIR FORCE SYSTEMS COMMAND
UNITED STATES AIR FORCE
HANSCOM AFB, MASSACHUSETTS 01731

84 11 26 007

This technical report has been reviewed and is approved for publication

RICHARD M. NADILE
Contract Manager

ADELBERT McINTYRE, Acting Chief
Atmospheric Backgrounds Branch

FOR THE COMMANDER

RANDALL E. MURPHY, Director
Infrared Technology Division

REPORT DOCUMENTATION PAGE

1a. REPORT SECURITY CLASSIFICATION	1b. RESTRICTIVE MARKINGS
Unclassified	

2a. SECURITY CLASSIFICATION AUTHORITY	3. DISTRIBUTION/AVAILABILITY OF REPORT
	Approved for public release;
2b. DECLASSIFICATION/DOWNGRADING SCHEDULE	distribution unlimited

4. PERFORMING ORGANIZATION REPORT NUMBER(S)	5. MONITORING ORGANIZATION REPORT NUMBER(S)
	AFGL-TR-83-0162

6a. NAME OF PERFORMING ORGANIZATION	6b. OFFICE SYMBOL (If applicable)	7a. NAME OF MONITORING ORGANIZATION
University of Cincinnati Physics Department		Air Force Geophysics Laboratory

6c. ADDRESS (City, State and ZIP Code)	7b. ADDRESS (City, State and ZIP Code)
Cincinnati, Ohio 45221	Hanscom AFB, Massachusetts 01731 Monitor/Richard Nadile/OPR-1

8a. NAME OF FUNDING/SPONSORING ORGANIZATION	8b. OFFICE SYMBOL (If applicable)	9. PROCUREMENT INSTRUMENT IDENTIFICATION NUMBER
		F19628-80-C-0138

8c. ADDRESS (City, State and ZIP Code)

10. SOURCE OF FUNDING NOS.

PROGRAM ELEMENT NO.	PROJECT NO.	TASK NO.	WORK UNIT NO.
61102F	2310	G4	AS

11. TITLE (Include Security Classification)
Analysis and Investigation of the (over)

12. PERSONAL AUTHOR(S)
Tai-Fu Tuan

13a. TYPE OF REPORT	13b. TIME COVERED	14. DATE OF REPORT (Yr., Mo., Day)	15. PAGE COUNT
Final Report	FROM 9/1/80 TO 8/31/83	1983 May 30	98

16. SUPPLEMENTARY NOTATION

17. COSATI CODES			18. SUBJECT TERMS (Continue on reverse if necessary and identify by block number)
FIELD	GROUP	SUB. GR.	(1) Analysis of Spatial and Temporal variability in Infrared radiance produced by gravity waves. (2) Development of dispersion relation for inhomogeneous atmosphere

19. ABSTRACT (Continue on reverse if necessary and identify by block number)

The effects of atmospheric gravity waves on the spatial and temporal variability of infrared radiance (IR), have been investigated, beginning with an analysis of the effects of such waves on the number densities of various minor species which produce the more important infrared radiance. The results show the following features. (1) The spatial structures produced by gravity waves depend strongly on the excitation mechanism for the minor species. If the excitation is local such as for the OH emissions, the structures in IR are sharply pronounced. If the excitation in integrated over extended sources, the structures are less sharply pronounced. (2) The temporal variance is far less influenced by the nature of the excitation. (3) The spatial structures increase with height. (4) Gravity waves with short vertical wave length compared to background structures produced both spatial and temporal variance in IR. (5) Gravity waves with long vertical wave length compared to background structures produce only temporal variance in IR. (6) Large amplitude gravity waves can produce instability and secondary IR structures with far more rapid→cont.

20. DISTRIBUTION/AVAILABILITY OF ABSTRACT	21. ABSTRACT SECURITY CLASSIFICATION
UNCLASSIFIED/UNLIMITED ☐ SAME AS RPT. ☐ DTIC USERS ☒	Unclassified

22a. NAME OF RESPONSIBLE INDIVIDUAL	22b. TELEPHONE NUMBER (Include Area Code)	22c. OFFICE SYMBOL

DD FORM 1473, 83 APR   EDITION OF 1 JAN 73 IS OBSOLETE.

cont →temporal variance as well as more pronounced spatial variance.

A dispersion relation for an inhomogeneous atmosphere has been developed for analyzing gravity waves and can be used even when there is heavy wave reflection. The relation reduces to the well-known Hines' dispersion relation in a homogeneous isothermal atmosphere.

Block 11 (Contd)   Effects of Atmospheric Gravity Waves on Infrared Emissions

TABLE OF CONTENTS

FINAL REPORT

Introduction

The principal objectives of this research program are to investigate the spatial and temporal variability in infrared (IR) radiance produced by atmospheric gravity waves. The investigations will be divided into the following four parts:

(1) The spatial and temporal variations in concentrations of [O], [NO], $[CO_2]$ and $[H_2O]$ produced by gravity waves for different exospheric temperatures corresponding to cases A, C, F, G and H in the AFGL report (AFGL-TR-81-0207).

(2) The spatial and temporal variations in the infrared volume emission rates of some of the above mentioned species.

(3) The development of a dispersion relation for analyzing short period gravity-wave induced infrared variance.

(4) The possible production of short-period (of the order of minutes) gravity-wave oscillations which can be either a primary wave or a secondary gravity wave produced by primary gravity waves with large amplitudes (20% or greater). Such basically horizontal "surface-like" waves occur often in the mesosphere with horizontal wave length in the tens of kilometers and horizontal phase velocities primarily in the few tens of meters per sec. These waves tend to produce very significant spatial and temporal variations in infrared radiance.

The possible connection between oscillations in atmospheric emissions and atmospheric waves was noted as far back as 1957 by Krassovsky (1957). Later, these effects were observed and analyzed by a number of investigators [e.g. Okuda, (1962); Silverman, (1962); Barbier, (1964, 1965); Weill and Christophe-Glaume, (1967); Dachs, (1968); Andrews, (1976); Dyson and Hopgood, (1978) for both the 6300A OI and the 5200 A NI. The presence of gravity waves in OH infrared

emissions has been examined by Krassovsky (1972), Krassovsky and Shagaev (1974,1977), Krassovsky et al (1977), Armstrong (1975) Moreel and Herse (1977) and Peterson (1979). Theoretical treatments for the effects of gravity waves on airglow have been made by Porter et al (1974) for 6300A OI and 5200 A NI and Hatfield et al (1981) for OH infrared emissions.

In general, the treatment of gravity-wave effects on airglow requires an analysis of the effects of gravity waves on the individual atmospheric constituents which produce the airglow. Thus, in part (1) we analyze the effects of gravity waves on the concentration of CO_2, NO, O and H_2O using the same basic technique developed by Hatfield et al (1981) for O_3. For gravity-wave models we use the models developed by Yu et al (1980). They were developed for the exospheric temperatures T_{ex} equal to 600^Ok, 1000^Ok, 1500^Ok, 1800^Ok and 2200^Ok, based on the 1972 COSPAR atmosphere. These gravity-wave models are particularly suitable for our purposes, since the exospheric temperatures correspond very closely to cases A (T_{ex} = 626.5^Ok), C(T_{ex} = 1081.2^Ok), F(T_{ex} = 1555.7^Ok), G(T_{ex} = 1829.4^Ok) and H(T_{ex} = 2176.8^Ok) that are being used in the AFGL report (AFGL-TR-81-0207).

For part (2) once the variations in the concentration profiles (produced by gravity waves) are obtained, the production of infrared emission from these species depend entirely on the mechanism which put the species in a particular excited state. For OH infrared emission, the primary mechanism is through chemical reactions, in particular the reaction between H and O_3 which produce the vibrationally excited OH molecules. For CO_2, NO, O and H_2O, the primary excitation mechanism is through collision (without reaction) and, above all, through absorption of radiation from different sources. In all optical emission calculations, the quantity we need to know is the concentration of excited states. Once this is found, the volume emission rate can be obtained, usually by assuming spontaneous emission and neglecting stimulated emissions. For low altitudes, the concentration

of excited states can be found through assuming chemical equilibrium (i.e. production rate of the excited states is set equal to the loss rate and both of which depend only on reaction rates). With this assumption, the concentration of excited states can be found algebraically. This method has been used in the AFGL Report (AFGL-TR-81-0207). At higher altitudes, however, we can no longer assume chemical equilibrium, since vertical diffusion may become important. With the addition of this effect to the loss rate, we end up with a second order self-adjoint differential equation for the concentration of excited states. The volume emission rate can be computed from this concentration by using the usual Einstein coefficients.

Of special importance to infrared radiance variance are the short period (of the order of minutes) waves or "ripples" which have pronounced spatial temporal variance. Such waves often (but not always) tend to behave like surface waves propagating horizontally with relatively low phase velocities (mostly less than 50 m sec^{-1}). These waves have been detected at 90 km by Peterson (1979) through their effects on OH emissions. To analyze these waves we need a dispersion relation which provides a formula for the vertical wave length, horizontal wave length and the frequency of gravity waves. Although there are numerical dispersion relationships available (for reference, see Hines (1974) and Francis (1975)) they are listed for a few definite gravity wave periods and horizontal phase velocities. Thus for general use there is only the analytic-formula of the Hines dispersion relation (1960) which is only valid for uniform isothermal atmosphere with no wave reflection. We are interested, on the other hand, in the inhomogenieties in spatial and temporal infrared radiance produced by gravity waves in the mesospheric region where the gravity-wave amplitudes grow to its maximum, while the sharp temperature rise at the base of the thermosphere produces heavy wave reflections. Furthermore, we are also interested in short-period gravity waves

- 3 -

with periods close to the Brunt period. It is therefore necessary to generalize
the dispersion relation to an inhomogeneous atmosphere which takes reflection
fully into account (see Papadopoulos et al (1982)) and remains valid as we approach
the Brunt frequency. Such a dispersion relation will be derived in this report
as part of part (3).

For part (4) we shall be primarily concerned with how a secondary short-
period oscillation or wave may be produced from a primary long-period wave.
Based on the fact that the velocity amplitude of a primary wave produced in the
lower atmosphere must grow with height until saturation of wave amplitudes occur
in the upper mesospheric region where, at least for the larger amplitude waves,
the Richardson's number turns negative and instability occurs.

Whilst a large variety of instability may occur in the atmosphere, it has
long been assumed that an important source of instability and atmospheric turbulence
in the mesospheric region may be due to the growth of gravity-wave velocity amplitudes
with height until Richardson's number falls below some critical value (Hodges
(1967); Hines (1974); Roper (1979); Zimmerman and Murphy, (1977); Manson and
Meek, (1980); Manson, Meek and Gregory, (1981)]. Saturation of gravity wave amplitudes
occur primarily above the mesospheric region where kinetic viscosity rises above
turbulence viscosity until eventually the kinetic viscosity damps out the gravity
wave mode at very high altitudes, (above 500 km). Since some important infrared
emissions such as the OH emission peaks in the mesospheric region, the instability
can produce large spatial and temporal variations in infrared radiance. For
part (4), we investigate, to lowest order, the production of a secondary short-
period oscillation from a primary long-period gravity wave. The instability
can produce turbulence and secondary oscillations closely associated with the
Brunt oscillation with frequencies and wave lengths which may be analyzed by
the dispersion relation derived in part (3).

- 4 -

Part (1)

(a) The Gravity Wave Model

In this part we consider the effect of gravity waves on the number density profiles of minor atmospheric constituents. We assume that the gravity waves are carried by the major atmospheric constituents and that the ambient atmosphere (including both major and minor components) is uniform along the horizontal directions (horizontal stratification). Using the theory developed by Tuan (1979) and Hatfield et al (1981), we can then show that

$$\Delta N = \frac{N_o k_x}{\omega} \Delta u_g + \frac{i}{\omega} \frac{\partial (N_o \Delta w_g)}{\partial z} \tag{1}$$

where N_o = concentration of the ambient minor atmospheric constituent

ΔN = perturbation amplitude of the minor atmospheric constituent

k_x = horizontal wave vector of the gravity wave

Δu_g = horizontal particle velocity of the gravity wave

Δw_g = vertical particle velocity of the gravity wave.

ω = frequency of the gravity wave.

The assumption of horizontal stratification for all perturbed physical quantities (i.e. ΔN, Δp, etc.) means that they may take on the generic form:

$$f(z)e^{i(\omega t - k_x x)} \tag{2}$$

where x is a horizontal co-ordinate. Furthermore, the gravity wave must satisfy Δw_g = o at the ground level, (the rigid surface boundary conditions). This means that we have a stationary wave along the vertical direction and that all the perturbed quantities must also be stationary along the vertical. Thus, f(z) is either pure real or pure imaginary. The imaginary number "i" in equation (1) comes from the complex notation we use and provides for the phase difference

- 5 -

between the first and the second terms.

For the gravity waves we use the model developed by Tuan (1976) and Yu et al (1980). The model expresses the horizontal and vertical velocity fields in terms of the pressure perturbation, Δp, as follows:

$$\Delta u_g = \frac{k_x}{\omega^2 \sqrt{\rho_o}} \psi \tag{3}$$

$$\Delta w_g = -\frac{i}{\sqrt{\rho_o} (\omega_b^2 - \omega^2)} [\frac{\partial \psi}{\partial z} - \lambda(z)\psi] \tag{4}$$

where $\quad \psi = \frac{\omega}{\sqrt{\rho_o}} \Delta p$

$$\lambda(z) = [\frac{\gamma g}{2c^2} + \frac{c'}{c} - \frac{g}{c^2}]$$

$\omega_b = \omega_b(z) = $ Brunt frequency

$\rho_o = $ ambient atmospheric density.

$c' = $ derivative of the speed of sound profile.

The rigid surface boundary condition requires that $\Delta w_g \bigg|_{z=o} = o$, so from (3) the corresponding condition on ψ is given by

$$\frac{\partial \psi}{\partial z}\bigg|_{z=o} = \lambda(o)\psi\bigg|_{z=o} \tag{5}$$

In this way, the horizontal and vertical velocity fields (Δu_g and Δw_g) can be both expressed in terms of the pressure perturbation ψ. It can be readily shown (Tuan (1976), Yu et al (1980) that ψ satisfied the following second order

self-adjoint hydrodynamic equation :

$$\left[\frac{d}{dz} Q \frac{d}{dz} - V + \Omega^2 \right]\psi = 0 \tag{6}$$

where

$$Q = \frac{1}{\omega_b^2(z) - \omega^2}$$

$$\Omega = \frac{k_x^2}{\omega^2} = \frac{1}{V_{phx}^2}$$

$$V(z,\omega) = \frac{1}{\omega_b^2 - \omega^2} \left\{ \left(\frac{c^2{}''}{c^2} \right) \left[\frac{1}{2} - \frac{1}{\omega_b^2 - \omega^2} \left(\frac{\omega_b^2}{2} - \frac{g^2}{2c^2} \right) \right] \right.$$

$$+ \left(\frac{c^2{}'}{c^2} \right) \left[\left(\frac{\omega_b^2}{2g} - \frac{g}{2c^2} \right) \frac{\omega_b^2}{\omega_b^2 - \omega^2} - \frac{1}{4} \left(\frac{c^2{}'}{c^2} \right) \right]$$

$$\left. + \frac{\omega_a^2 - \omega^2}{c^2} \right\}$$

$$\omega_a^2 = \left(\frac{\gamma g}{2c} \right)^2 + g \left(\frac{c^2{}'}{c^2} \right) = \text{acoustic cut-off frequency}$$

$$\omega_b^2 = \frac{(\gamma - 1)g^2}{c^2} + g \left(\frac{c^2{}'}{c^2} \right) = \text{Brunt frequency.}$$

Equation (6) is identical to the usual coupled hydrodynamic equations in the absence of dissipation. It is possible through elimination of the other variables such as the density $\Delta\rho$, the horizontal velocity Δu_g and the vertical velocity Δw_g to obtain equation (6) for ψ which is proportional to the pressure perturbation Δp.

Although both Q and V in equation (6) depend on the frequency, for any gravity wave with period greater than 30 minutes Q and V become essentially independent

of frequency. Since most gravity waves found in nature tend to have periods of the order of one to two hours (Battaner & Molina (1980)), we may neglect the variations with frequency of Q and V.

To calculate Q and V Tuan (1976) and Yu et al (1980) have used the 1972 COSPAR model for the temperature profile, the mean molecular mass, the ratio of specific heats. The variation in the acceleration due to gravity is of course very easily taken care of. For the present report we have used 5 different exospheric temperatures. They are $600^{\circ}k$, $1000^{\circ}k$, $1500^{\circ}k$, $1800^{\circ}k$ and $2200^{\circ}k$. These temperatures taken from COSPAR (1972) are the closest approximations we can find to cases A $(626.5^{\circ}k)$, $C(1081.2^{\circ}k)$, $F(1555.7^{\circ}k)$, $G(1829.4^{\circ}k)$ and $H(2176.8^{\circ}k)$ in the AFGL Report (AFGL-TR-81-0207).

We have used gravity wave models with different horizontal phase velocities corresponding to different vertical wave lengths. In general, it is the vertical wave lengths that produce the spatial variations in infrared radiance, but the vertical wave length varies with height in our inhomogeneous atmosphere. So the horizontal phase velocity, $V_{phx} = \dfrac{\omega}{k_x}$, whose inverse is just Ω, the square root of the eigenvalue in equation (6) and can therefore be used to designate the type of gravity wave we use. In general, a smaller vertical scale structure implies a smaller vertical wave length which in turn implies a smaller horizontal phase velocity. From the paper by Tuan (1976) and Yu et al (1980) we can show that there are two types of gravity waves. One type has a large horizontal phase velocity (greater than 400 m sec^{-1}) with its energy primarily concentrated in the F-region (above 110 km). Such waves do not significantly effect the lower altitudes where some of the more important infrared emission profiles peak. The second type has a low horizontal phase velocity (less than 400 m sec^{-1}) with much of its energy concentrated in the lower atmosphere. It is such waves which have a strong effect on infrared emission that we use as gravity wave models.

The particular choices of gravity wave horizontal phase velocities are based on the frequency of occurrence of typical gravity-wave velocities. Battaner and Molina (1980) have found that the horizontal phase velocities typically range from 60 to 140 m sec^{-1}. Since the more pronounced vertical scale structures are produced by gravity waves with low horizontal phase velocities, we choose two horizontal phase velocities for our gravity-wave models in the lower end of the typical range, 60 and 78 m sec^{-1}. We also choose a horizontal phase velocity of 129 m sec^{-1} for case F. Our gravity wave model is valid up to 120 km. Above 120 km, dissipation due to molecular viscosity and heat conduction gradually become significant and the models cannot be used without modification.

(b) Spatial variations of minor atmospheric constituents

In this section we consider the effects of gravity waves on the concentration profiles of the following atmospheric constituents associated with infrared emission: (1) Day [O]; (2) Night [O]; (3) Day [NO]; (4) Night [NO]; (5) [CO$_2$]; (6) [H$_2$O]. For each ambient profile we computed the perturbation amplitude ΔN from equation (1) in which we substitute each of the above six profiles for N_o in turn. Δu_g and Δw_g, the gravity wave velocities are computed from equation (3), (4) and (6) for the exospheric temperatures mentioned in part (a) which correspond to the 5 cases A, C, F, G and H in the AFGL Report. Table I provides the key to the graphs for the ambient and gravity-wave perturbed profiles.

Fig. 9 to 38 (inclusive) show the calculations for Day [O], Night [O], Day [NO], Night [NO], [CO$_2$] and [H$_2$O] profiles under the influence of gravity waves with horizontal velocities of 60 to 78 m sec^{-1}. For such horizontal phase velocities, the vertical wave length is small compared with the structure scale sizes of the unperturbed atmospheric constituent. The spatial variations in the profile imposed by the gravity wave show up rather dramatically. This would not be true

TABLE I

	Unperturbed density profile	G.W. Perturbed density profile	Horizontal Phase Velocity for G.W. in m sec^{-1}					
Case	Exos. Temp. $^{\circ}$k	Exos. Temp. $^{\circ}$k	Day [0]	Night [0]	Day [NO]	Night [NO]	[CO$_2$]	[H$_2$0]
A	626.5	600	60	60	60	60	60	78
C	1081.2	1000	78	78	60	60	60	78
F	1555.7	1500	79 129	78 129	60 129	60 129	60 129	78
G	1829.4	1800	78	78	60	60	60	78
H	2176.8	2200	78	78	60	60	60	78

for a gravity wave with large horizontal phase velocity and hence greater vertical wave length. If the vertical wave length becomes large compared with the scale size of the background atmospheric structure, no spatial variations can be detected as we will show in the next section.

In Figure 4, 5, 6, 7 and 8 we examine what happens when an intermediate horizontal phase velocity (v_{phx} = 129 m sec^{-1}) with an effective larger vertical wave length is used. The results show some vertical structures. The structure produced in the CO$_2$ profile (Fig. 2) occurs at about 110 km and bears some resemblance to the SPIRE data (14.05 - 16.0 µm). Owing to the natural growth of wave amplitudes with height, there should be more prominent structures at higher altitudes. However, due to the rapid increase in molecular viscosity above 110 km, there should be considerable damping of wave amplitudes above 120 km leaving the most prominent oscillation at almost 110 km. But even with all the dissipation included, it is difficult to see how all traces of oscillation

can immediately cease above 110 km as the SPIRE data seems to show. In fact, the damping of a gravity wave does not become total until above 500 km. Thus, in the absence of further experimental evidence, we feel we may continue to support our previous conclusion given in the "Assessment on CO_2 (ν_2) Radiance Profile," by Chow and Tuan (1980).

(c) Temporal variations

In order to investigate the temporal variability of infrared radiance produced by gravity waves, we have considered (1) the case in which the vertical gravity wave length is less than the background atmospheric structure and simultaneous spatial and temporal variations may be observed; (2) the cases in which the vertical wave length is long compared with background structure and as a result spatial variations can no longer be easily detected but temporal variations continue to be very readily observable. In (2) we consider the special case of the guided Lamb mode with a horizontal phase velocity of over 300 m sec^{-1} and a rather long vertical wave length. The choice of periods for the gravity waves is dictated by typical values. Most frequently observed gravity waves have a period of between 2 and 3.5 hours (Battaner et al, (1977)). We have chosen a gravity wave with a period of 2 hours.

The results for (1) mentioned above are shown in Fig. 1a, 1b, 1c and 1d where profiles for Day [0] are given for T = 0, 0.25, 0.5, 0.75 and 1 hour respectively for a gravity wave with a 2 hour period and a horizontal phase velocity of 78 m sec^{-1}. Since the vertical wave length for such a wave is small compared with the scale size of the background [0] structure, we see considerable simultaneous spatial and temporal variations. In Fig. 2 we see what happens to the same profile when the horizontal phase velocity is close to a guided mode, in particular, the Lamb mode. For such a mode the vertical wave length is long compared to

- 11 -

the scale size of the ambient profile structure and we see that the profile shape

is unaffected by the wave. Instead, the whole profile oscillates up and down

at T = 0 and 1 hour for a gravity wave with a 2-hour period. The only infrared

variance associated with atomic oxygen that may be observed will be through the

ground-based photometers which would show a periodic oscillation in the total

zenith intensity. This would be the results for (2) mentioned above where spatial

variations is all but unobservable and one can only observe the temperal changes.

Fig. 3 shows the same type of phenomena for Day [NO] profile

Part (2)

The infrared volume emission rate profiles are calculated from the concentration

profiles mentioned in part (1) by assuming that all such emissions come from

spontaneous emission of vibrationally excited states of $[O]$, $[NO]$, $[CO_2]$ and

$[H_2O]$ (See AFGL Report). The problem therefore reduces to the determination

of the concentration of vibrationally excited states. For some infrared emitters

such as [OH] the principal excitation mechanism is through its chemical formation

$(H + O_3 \rightarrow OH^* + O_2)$ which leaves it in an excited vibrational state. For the

minor atmospheric constituents we treat here in this report, the principal excitation

mechanism is through absorption of infrared radiation. Such absorption can come

from three different radiation sources: (1) the radiation from the lower

atmospheres considered as a plane blackbody; (2) the direct solar radiation;

(3) the radiation from other atoms and molecules in the atmosphere. Since all

three radiation sources have to pass through a certain thickness of atmosphere

before they reach the height level z where we compute the concentration of excited

states, we need to use the well-known radiative transfer functions to take care

of the loss of intensity of the radiations as they traverse from their source

through the atmosphere to reach the point at z. Such radiative transfer functions

are not necessary for OH infrared emission since its principal excitation mechanism is through local chemical reactions rather than through radiation sources from far away.

Once the excitation rate is computed, the concentration of each particular excited state may be determined through assuming chemical equilibrium (AFGL Report). Thus, if [X] is the concentration of the minor species which emit infrared radiation and $[X]^*$ is the concentration of a particular vibrationally excited state and [Y] and [Z] are concentrations of any two gases which collide with [X] and $[X]^*$ respectively, we may write the equation for chemical equilibrium

$$\alpha[X][Y] + B[X] = \beta[X]^*[Y] + A[X]^* \tag{7}$$

where α = rate coefficient for collisional excitations

   B = radiative excitation coefficient and is calculated from the radiative transfer functions.

   β = rate coefficient for collisional de-excitation

   A = Einstein coefficient for spontaneous radiation of $[X]^*$.

Equation (7) essentially assumes that production rate of excited states is equal to the loss rate and is sufficiently accurate at altitudes up to 200 km. It is an algebraic equation from which the concentration of excited states [X] can be readily solved.

At higher altitudes, however, there is an additional loss rate through vertical diffusion which is neglected in the calculations in AFGL Report (AFGL-TR-81-0207) and which may be important. To take this into account we have to write down the following mass and momentum conservation equation for $[X]^*$:

$$\frac{\partial[X]^*}{\partial t} = \alpha[X][Y] + B[X] - \beta[X]^*[Z] - A[X]^*$$

$$- \text{div}\{[X]^* v_d\} \tag{8}$$

$$m[X]^* v_d \nu = -\frac{\partial p}{\partial z} - m[X]^* g \qquad (9)$$

$$p = [X]^* kT \qquad (10)$$

where ν = collision frequency with other molecules

p = partial pressure of $[X]^*$

v_d = vertical drift velocity

In equation (8), we may assume quasi-equilibrium (i.e. $\frac{\partial [X]^*}{\partial t} = 0$). This assumption was also made in the AFGL Report. From equations (9) and (10) we obtain

$$\ddot{v}_d = -\left(\frac{kT}{m\nu}\right) \frac{1}{[X]^*} \frac{\partial [X]^*}{\partial z} - \frac{g}{\nu}$$

$$= -D \left[\frac{1}{[X]^*} \frac{\partial [X]^*}{\partial z} + \frac{1}{H} \right] \qquad (11)$$

where $D = \frac{kT}{m\nu}$ = the diffusion coefficient for $[X]^*$

$H = \frac{kT}{mg}$ = scale height for $[X]^*$

In deriving (11) we have assumed that the kinetic temperature in nearly constant above 200 km where the diffusion term becomes important. Substituting (11) in (8) and setting $\partial [X]^*/\partial t = 0$, we obtain

$$\frac{\partial}{\partial z} D \left[\frac{\partial}{\partial z} + \frac{1}{H} \right] [X]^* - (A + \beta[z])[X]^* + \alpha[X][Y] + B[X] = o \qquad (12)$$

Quite obviously equation (12) reduces to equation (7), the equation for

chemical equilibrium when we neglect the diffusion (i.e. setting D = 0). Unlike

(7) equation (12) is a second order self-adjoint differential equation and requires

more work to obtain $[X]^*$, the concentration of the excited states.

The physical reason why the diffusion term is important is that the diffusion

coefficient is inversely proportional to the collision frequency. At higher

altitudes, there will be a rapid decrease in the collision frequency, thus producing

a large increase in D(z). Such an increase in vertical diffusion will result

in an increased in $[X]^*$ at higher altitudes.

Fig. 39 to 44 (inclusive) show the effect of gravity waves with a horizontal

phase velocity of 78 m sec^{-1} on both the day time and the night time infrared

emission rate profiles of [NO]. We have shown only the $1 \rightarrow 0$ vibrational transition

with a band center at 5.325 μm. It is interesting to compare these results with

Fig. 11, 12, 21, 22, 31 and 32 which show the effect of gravity waves on the

concentration profiles. It is obvious that the variations are greater in the

concentration profiles than they are in the emission profiles. The physical

reasons for this are easily understood. For [O], [NO], $[CO_2]$ and $[H_2O]$ the excited

states are produced principally by the absorption of radiation from three different

sources; the infrared radiation form the lower atmosphere considered as a plane

blackbody; the direct solar radiation; the radiation from the rest of the atmosphere.

The latter effect has to be integrated over the entire height range of the atmosphere

and has a significant smoothing effect.

There are other types of infrared emissions such as OH emissions, for instance,

in which the principal excitation mechanism is through local chemical reaction

(i.e. $H + O_3 \rightarrow OH^* + O_2$) and there is no "smoothing" of the emissions profile

from an integration over the height range of the atmosphere. The production

of excited OH states are then completely local and the emission profiles can

exhibit far more pronounced spatial structure. This can be seen from the computed

- 15 -

profiles of Hatfield et al (1981) in which the magnitude of the variations in
the spatial structures of the emission profiles are comparable to the corresponding
variations in the concentration profiles.

Part III

To analyze the more sharply pronounced spatial and temporal structure with
scale sizes of the order of a few tens of kilometers and a few minutes, we need
to develop a dispersion relation for the short period gravity waves with frequencies
close to the Brunt frequency. Since such spatial and temporal inhomogenieties
tend to occur in the mesospheric region where variations in the temperature and
mean molecular mass of the ambient atmosphere as well as the possibility of heavy
wave reflection from the sharp temperature rise in the base of the thermosphere
require drastic modifications to the Hines' dispersion relation (Hines, (1960);
Eckart, (1960)). Actually, generalizations of this dispersion relation to an
inhomogeneous but horizontally stratified atmosphere including dissipation has
been made in thw WKB approximation, (Pitteway & Hines (1963), Midgley and Liemohn
(1966), Yeh and Liu (1974), Francis (1975)).

It is the purpose of the present paper to analyze a generalization of Hines'
dispersion relation to an inviscid but inhomogeneous and horizontally stratified
atmosphere which remains valid not only for free modes, but also for guided or
partially guided modes. In the derivation we use methods and techniques based
on a "potential" treatment of gravity waves (Tuan (1976), Yu et al (1980), Tuan
and Tadic (1982)). The generalized dispersion relation would retain a relatively
simple analytic form and can hence be easily used to estimate wave lengths, frequencies
or horizontal phase velocities as the case may be as well as to provide simple
qualitative estimates of the limits of validity of the Hines' dispersion relation.
To accomplish this, we begin by examining how a vertical wave vector and hence

a "local" vertical wave length can be meaningfully defined in an inhomogeneous atmosphere. Two specific cases will be studied. One case will deal with gravity waves with frequencies close to the Brunt and acoustic cut-off frequency while the other case deals with long period gravity waves. For the former case we will show that in altitude ranges where $\omega_b(z) \rightarrow \omega$, the "local" vertical wave vector will always be very large and pure imaginary. For the latter case we will examine the variation of horizontal phase velocity with height for zero vertical wave vector. From such a curve, one can identify a region of horizontal phase velocities in which the Hines' relation is valid. Such a curve will also show for a fixed horizontal phase velocity the height ranges in which the Hines' dispersion relation is valid.

In the appendix we will work out the lower frequency limit as well as the height range in which the generalized dispersion relation can be be used.

(a) Method and definition of "local" wavelength

In an inviscid inhomogeneous and horizontally stratified atmosphere, the linearized hydrodynamic equations for monochromatic wave solutions are given by

$$i\omega\Delta\rho = ik_x\rho_0\Delta u - \frac{\partial}{\partial z}(\rho_0\Delta w) \qquad (13)$$

$$i\omega\rho_0\Delta u = ik_x\Delta p$$

$$i\omega\rho_0\Delta w = -g\Delta\rho - \frac{\partial(\Delta p)}{\partial z}$$

$$i\omega\Delta\rho = \frac{i\omega}{c^2}\Delta p + \frac{\rho_0\omega_b^2(z)}{g}\Delta w$$

where $\Delta\rho$, Δu, Δw and Δp are respectively the density, horizontal velocity, vertical velocity and pressure perturbations, $\omega_b(z)$ is the Brunt frequency. ω is the

gravity wave frequency. k_x is the horizontal wave vector, and c is the speed of sound profile. Tuan and Tadic (1982) have shown that equation (13) can be transformed into the following Sturm-Liouville equation for the pressure perturbation without approximations,

$$\left[\frac{d^2}{dz^2} - V + W^2 k^2 \right] \Phi = 0 \tag{14}$$

where $\Phi = \left[\dfrac{\omega_b^2(a) - \omega^2}{(\omega_b^2(z) - \omega^2)\rho_0} \right]^{\frac{1}{2}} \Delta p$

a = some upper boundary above which the atmosphere may be assumed to be uniform.

$$k^2 = k_z^2 = \frac{\omega_b^2(a) - \omega^2}{\omega^2} k_x^2 - \frac{\omega_a^2 - \omega^2}{c^2(a)} \tag{15}$$

In equation (14), $V(a) = 0$ and $W(a) = 1$. Thus, above the upper boundary, Φ has only plane wave solutions. Below the upper boundary $V(z)$ and $W(z)$ are well-behaved functions of z as well as the parameter ω, (Their explicit forms are given by eqution (10) in the paper by Tuan and Tadic (1982)).

Equation (13) may be put into the form:

$$\left[\frac{d^2}{dz^2} + \overline{K}_z^2 (z) \right] \Phi = 0 \tag{16}$$

In this form Φ may be considered as a solution of a wave equation with local wave vector $\overline{K}_z$ and local wave length $\dfrac{2\pi}{\overline{K}_z}$.

To see this from another point of view we can divide the atmosphere up into thin uniform horizontal slabs such that V and W are constant within each slab. This means of course that $\overline{K}_z(z)$ is also constant within each slab. Thus, the solutions in the i th slab with thickness Δz are given by:

$$\Phi(z) \sim e^{\pm i \, \overline{K}_z(z_i) \, z} \tag{17}$$

These solutions in (17) are obviously plane wave solutions with vertical wave length $\lambda_{zi} = \dfrac{2\pi}{\overline{K}_z(z_i)}$. We can construct the entire solution for all z by imposing boundary conditions at the ground and the upper boundary as well as suitable interfacial boundary conditions between slabs. In this way the local wave length λ_z may be defined by shrinking the slab to very small thickness so that

$$\lambda_z = \lim_{\Delta z_i \to 0} \lambda_{zi} .$$

This approach is quite different from the usual multi-layer method such as the one used by Volland (1969) in that the slabs are not necessarily uniform in temperature or mean molecular mass but are uniform in the quantities $V(z)$ and $W(z)$ which have been previously identified as "potentials" in analogy with the Schrodinger equation (Yu et al (1980), Tuan and Tadic (1982)). Thus, instead of isothermal slabs, we have essentially "isopotential" slabs. The difference between the isopotential and the isothermal slab is that <u>all</u> height derivatives of atmospheric parameters (such as temperature, background density etc) are automatically included in the isopotential slabs.

Here we wish to emphasize that the local wave length we have used is exact and not derived through a WKB type of approximation.

By substituting the expressions for $V(z)$ and $W(z)$ (taken from equation (10), Tuan and Tadic (1982)) we can show that

$$\overline{K}_z^{\,2}(z) = \left[\frac{\omega_b^{\,2}(z) - \omega^2}{\omega^2} k_x^{\,2} - \frac{\omega_a^{\,2}(z) - \omega^2}{c^2} \right]$$

$$+ \, \xi_o(z) + \frac{\xi_1(z)}{\omega_b^{\,2}(z) - \omega^2} - \frac{\xi_2(z)}{(\omega_b^{\,2}(z) - \omega^2)^2} \tag{18}$$

- 19 -

where $\xi_0(z) = [\frac{1}{4}(\frac{c^{2'}}{c^2})^2 - \frac{1}{2}\frac{c^{2''}}{c^2}]$

$$\xi_1(z) = \frac{1}{2}\{[\frac{c^{2''}}{c^2} - \frac{c^{2'}}{c^2}\frac{\omega_b^2}{g}](\omega_b^2 - \frac{g^2}{c^2}) + \frac{d^2(\omega_b^2)}{dz^2}\}$$

$$\xi_2(z) = \frac{3}{4}(\frac{d(\omega_b^2)}{dz})^2$$

$$\omega_b^2(z) = -g[\frac{1}{\rho_o}\frac{d\rho_o}{dz} + \frac{g}{c^2}] = \text{Brunt frequency}$$

$$\omega_a^2(z) = (\frac{\gamma g}{2c})^2 + g(\frac{1}{c^2}\frac{dc^2}{dz}) = \text{acoustic cut-off frequency;}$$

and all primes on the speed of sound profile $c(z)$ denote height derivatives.

It is obvious that for an uniform isothermal atmosphere $\xi_0 = \xi_1 = \xi_2 = 0$ and equation (18) immediately reduces to the Hines' dispersion relation given by the bracket term on the right-hand side of (18). It is interesting to note that since ξ_o, ξ_1 and ξ_2 depend only on the background atmosphere and do not depend on the gravity-wave parameters, at low frequencies ($\omega \ll \omega_b$), all three correction terms to the Hines' relation become independent of the gravity-wave frequency. Thus, if the period is long, the Hines' relation is true only for small horizontal phase velocity for which the first term on the right-hand-side of equation (18) dominates.

For short-period gravity waves the most interesting term in equation (18) is the last term on the right-hand side. Quite obviously, for any horizontal phase velocity, as $\omega_b \to \omega$ the last term on the right-hand side of (18) dominates. Since $\xi_2(z) > 0$ for all z and the denominator is always positive, this term is always

- 20 -

negative. This also means that at those height levels where $\omega_b(z) \sim \omega$, $\overline{\underline{K}}_z$ is always pure imaginary and very large. Hence, the wave is always purely evanescent and the amplitude drops to zero very quickly. To see this we consider the "potential" (Tuan 1976, Yu et al (1980)) for a gravity wave with a 7.5 minute period, (Fig. 45). Quite obviously at approximately 160 to 170 km there is a sharp infinite potential barrier produced by the vanishing of the denominator $\omega_b^2(z) - \omega^2$. Within this barrier $\overline{\underline{K}}_z$ is infinite and pure imaginary and there is no wave propagation within this region. Above this region $\omega_b^2 < \omega^2$ and only acoustic waves can propagate. The infinite potential barrier therefore separates the gravity-wave mode from the acoustic-wave mode. This can be seen in Fig. (46) in which a 7.5 minute period wave would cut the Brunt period T_b at 163 km where the "potential" rises to infinity. At 167 km it intersects with the acoustic cut-off period so that above 167 km acoustic wave propagation is permissible. Since we have identified $\overline{K}_z$ as the vertical wave vector, we shall from now on refer to both $\overline{\underline{K}}_z$ and k_z as simply k_z.

(b) Application of dispersion relation and comparison with the Hines' relation

To facilitate the use of the dispersion relation (18), we have provided a table (Table II) for the function ω_b^2, ω_a^2, c^2, ξ_0, ξ_1 and ξ_2 at 5 km intervals from the ground level up to 120 km. Since ξ_0, ξ_1 and ξ_2 depend on derivatives of atmospheric parameters, the results are exceedingly sensitive to the model atmosphere. We have used the Winter mid-latitude COSPAR 1972 model. Great care must be taken in smoothing a curve for further numerical differentiation, since this often results in shifting the phase of the differentiated curve. We have adopted the inverse procedure of smoothing the differentiated curve and integrating to verify that we obtain the same original curve.

We compare equation (18) with the Hines' dispersion relation for two cases. One for $\omega \sim \omega_b$ and the other for $\omega \ll \omega_b$. In Fig. 46 there are three vertical

- 21 -

lines corresponding to gravity-wave periods T = 3.75, 4.6 and 6.1

minutes. These lines either come close to or intersect with the Brunt period

at different altitudes. At such altitudes $\omega \sim \omega_b$ and two out of the three corrections

to the Hines' dispersion relation become important. Table III shows the values

of k_z as calculated by the Hines' relation and equations (4) at the above altitudes.

The values of k_x are so chosen that k_z^2 is either immediately above or below

zero, (i.e. close to the turning point of the WKB approximation).

In general, one would expect the Hines' relation as well as the WKB approximation

to become very inaccurate close to such turning points. As can be seen from

Table III there is an enormous difference between k_z^2 obtained from (16) and

the Hines' relation.

For very much larger gravity-wave periods (such as 120 minutes) we may neglect

ω^2 in comparison with ω_b^2 or ω_a^2 and the corrections to the Hines' relation can

continue to be important for values of k_z^2 close to zero but are in general much

smaller. Table III again shows the significant albeit much smaller difference

between the values of k_z^2 obtained from (18) and from the Hines' relation. For

all long period gravity waves the correction to the Hines' relation does not

arise as a result of the vanishing of the denominator $(\omega_b^2 - \omega^2)$, but as a result

of large enough horizontal phase velocities for which the Hines' relation in

the bracket term of (18) is all but cancelled by the three correction terms which

no longer depend on gravity-wave parameters.

Fig. 47 shows a plot of $V_{phx}^2(k_z^2 = 0)$ against altitude for large period

gravity wave. From (18) and the assumption $\omega^2 << \omega_b^2$, we obtain:

$$V_{phx}^2(k_z^2 = 0) = \frac{\omega_b^2}{(f)} = V_{phx,o}^2 \tag{19}$$

TABLE II

z(km)	ω_b^2 (sec^{-2}) 10^{-3}	ω_a^2 (sec^{-2})	c^2 (km^2 sec^{-2}) 10^{-1}	ξ_o (km^{-2}) 10^{-2}	ξ_1 (km^{-2} sec^{-2}) 10^{-5}	ξ_2 (km^{-2} sec^{-4}) 10^{-9}
0.0	0.515	0.591 x 10^{-3}	0.987	0.124	0.155	+0.600
5.0	0.326	0.403	0.978	0.066	0.041	+0.055
10.0	0.325	0.406	0.919	0.018	-0.005	+0.010
15.0	0.353	0.440	0.853	-0.043	-0.053	+0.165
20.0	0.626	0.678	0.842	-0.116	-0.142	+1.521
25.0	0.608	0.643	0.907	-0.002	-0.021	+0.003
30.0	0.543	0.619	0.952	0.023	-0.019	+0.022
35.0	0.508	0.580	1.002	0.018	0.005	+0.042
40.0	0.467	0.535	1.044	0.028	0.018	+0.049
45.0	0.425	0.491	1.072	0.035	0.025	+0.044
50.0	0.387	0.452	1.082	0.035	0.030	+0.033
55.0	0.355	0.421	1.073	0.034	0.324 (10^{-6})	+0.019
60.0	0.332	0.398	1.046	0.030	0.317	+0.006
65.0	0.321	0.390	1.002x	0.022	0.306	+0.035 (10^{-12})
70.0	0.327	0.399	0.947	0.009	0.276	+0.007 (10^{-9})
75.0	0.353	0.430	0.888	-0.009	0.171	+0.038
80.0	0.402	0.482	0.833	-0.035	0.032	+0.104
85.0	0.469	0.553	0.799	-0.063	-0.016	+0.188
90.0	0.553	0.638	0.793	-0.089	-0.027	+0.169
95.0	0.603	0.683	0.816	-0.109	-0.039	+0.075
100.0	0.667	0.741	0.879	-0.122	-0.073	+0.107
105.0	0.708	0.772	1.000	-0.114	-0.092	+0.015
110.0	0.707	0.760	1.190	-0.082	-0.076	+0.013
115.0	0.667	0.711	1.448	-0.045	-0.052	+0.084
120.0	0.580	0.614	1.882	-0.007	-0.036	+0.143

T A B L E III

T (min)	z (km)	k_x (km^{-1})	k_z^2 (km^{-2}) (Hines' relation)	k_z^2 (km^{-2}) (Hines rel. plus corrections)
3.75	20	.07	0.245×10^{-3}	0.492×10^{-1}
		.08	-0.506×10^{-4}	0.489×10^{-1}
	105	.02	0.388×10^{-4}	0.146×10^{-1}
		.03	-0.744×10^{-5}	0.145×10^{-1}
4.6	19	0.11	-0.198×10^{-3}	0.359
		0.12	0.14×10^{-3}	.36
	31	0.16	-0.434×10^{-4}	0.681×10^{-1}
		0.17	0.769×10^{-4}	0.682×10^{-1}
	90	0.15	-0.987×10^{-5}	0.123
		0.16	0196×10^{-3}	0.123

T (min)	z (km)	k_x (km^{-1})	k_z^2 (km^{-2}) (Hines relation)	k_z^2 (km^{-2}) (Hines relation plus correction)
6.1	7	0.11	-0.733×10^{-4}	0.32×10^{-2}
		0.12	0.117×10^{-3}	0.339×10^{-2}
	66	0.1	-0.801×10^{-4}	0.12×10^{-1}
		0.11	0.105×10^{-3}	0.122×10^{-1}
120	7	0.01	0.377×10^{-1}	0.381×10^{-1}
	19	0.01	0.698×10^{-1}	0.667×10^{-1}
	20	0.01	0.741×10^{-1}	0.75×10^{-1}
	31	0.01	0.64×10^{-1}	0.64×10^{-1}
	66	0.01	0.381×10^{-1}	0.392×10^{-1}
	90	0.01	0.644×10^{-1}	0.636×10^{-1}
	105	0.01	0.851×10^{-1}	0.827×10^{-1}
	140	0.01	0.435×10^{-1}	0.436×10^{-1}

where $f(z) = \dfrac{\omega_a^2(z)}{c^2} - \xi_o(z) - \dfrac{\xi_1(z)}{\omega_b^2} + \dfrac{\xi_2(z)}{(\omega_b)^4}$

For any k_z^2 we can write

$$k_z^2 = \frac{\omega_b^2}{V_{phx}^2} - \frac{\omega_b^2}{V_{phx,o}^2} \tag{20}$$

To take a specific example, we shall assume that the criterion just mentioned is satisfied if $V_{phx}^2 \leq \frac{1}{10} V_{phx,o}^2$. Then we just simply draw the curve $V_{phx}^2 = \frac{1}{10} V_{phx,o}^2$ and we know that in the shaded region below this curve the first term on the right-hand side of (8) which is the important term in the Hines' relation is at least 10 times greater than the "correction" to the Hines' relation. Hence, we may well expect that within this shaded region, the Hines relation is a good approximation.

On the other hand, if we decide that for V_{phx}^2 to be in the range $\frac{1}{2} V_{phx,o}$ $> V_{phx}^2 > \frac{1}{10} V_{phx,o}^2$. The Hines' relation is good enough, we can draw in the curve $V_{phx}^2 = \frac{1}{2} V_{phx}^2$, $_0$ and assume that within this region the Hines' relation is say fair to good. For $V_{phx}^2 > \frac{1}{2} V_{phx,o}^2$. The Hines' relation is obviously not particularly good.

As an example of how one may make use of Fig. 47 we consider a long-period gravity wave with a horizontal phase velocity of 200 m sec^{-1}. We draw a horizontal line in Fig. 47 for $V_{phx}^2 = 0.04$ km^2 sec^{-2}. We see that between 30 km and 77.5 km as well as above 109 km the horizontal phase velocity falls within the region $\frac{1}{2} V_{phx,o}^2 > V_{phx}^2 > \frac{1}{10} V_{phx}^2$ within which the Hines' relation is fair to good. It should not be used at the other height ranges. Here we should emphasize that the numbers 1/2 and 1/10 are chosen purely arbitrarily to illustrate our point.

Clearly the curve $V_{phx}^2 = V_{phx,o}^2$ separates the region $k_z^2 > 0$ from the region $k_z^2 < 0$. Thus, above this curve the gravity wave becomes evanescent. Our dispersion relation given by (6) remains valid for all these regions. We can hence use Fig. 47 to determine the regions in the atmosphere in which a long-period gravity wave with a given horizontal phase velocity may be evanescent. As an example, we consider a gravity wave with a horizontal phase velocity of say 346 m sec^{-1}. This means $V_{phx}^2 = 0.12$ km^2 sec^{-2}. The horizontal line for this phase velocity in Fig. 47 shows that the wave is evanescent everywhere except in a narrow region between 44 and 64 km. We see also that the wave can propagate above 116 km.

Part (4)

Whilst a large variety of instabilities may occur in the atmosphere, it has long been known that an important source of atmospheric instability and turbulence in the mesospheric region may be caused by the growth of gravity-wave velocity amplitudes with height until Richardson's number falls below some critical value [Hodges, 1967; Hines, 1974; Roper, 1977; Zimmerman and Murphy, 1977; Manson and Meek, 1980; Manson et al (1981)]. It is also well known that important optical emissions, such as the 5577A OI and the OH infrared emissions, also peak in the same region (i.e. between 80 km and 100 km).

Ground-based photometric measurements have shown that in the presence of a gravity wave the 5577A OI emission often exhibits a short period oscillation (of the order of minutes) superimposed on a long period gravity-wave oscillation [Okuda 1962; Silverman, 1962; Tuan et al., 1979]. OH airglow photographs by Peterson and Kieffaber from 1972 onward show an extremely wide variety of moving and stationary airglow structures, some of which vary in brightness [Peterson and Kieffaber, 1973; Peterson, 1979]. Parallax measurements from the ground and

from aircraft place these features at heights of 80 to 100 km [Peterson and Kieffaber, 1973; 1975]. Of particular interest are airglow features of extremely short wavelength and short time duration which we have called "ripples". These "ripples" (1) have a very uniform wavelength of the order of ten kilometers; (2) have a constant horizontal velocity which can have values from 0 to 100 m/s; (3) have periods of the order of a few minutes; (4) appear suddenly and fade with a lifetime of about 45 minutes; and (5) sometimes appear to be at a different height from, and exhibit relative motion with respect to, the large-scale background airglow structures. In addition we have found that the time of occurrence of ripples is very well correlated with lower lunar transit (LLT). Fig. 49 shows this correlation.

During her thesis work, Kieffaber [1973] made many all-sky maps at 1.65 μ and 2.15 μ while Peterson photographed the sky in the near infrared. Fig. 48 shows an all-sky map for the night of 2 December 1972. Darker areas represent higher intensity of OH emission. On this night ripples were photographed in the brightest region of OH emission, in the southwest part of the sky. Lunar transit occurred at 2105 MST, near the middle of the mapping period, and the ripples were photographed at 2130 MST.

In general, gravity-wave oscillations observed through optical emissions are divided into two types. One type shows a relatively smooth oscillation with a period of the order of hours , [Dachs, 1968]. The second type shows a long period oscillation with a short period oscillation of the order of minutes superimposed. Figures 50 and 51 are examples of these second types of waves. The small period oscillations usually occur only in the presence of large amplitude gravity waves. The superimposed short period oscillation may appear gradually as a self-excitation, or it may appear more violently.

Battaner & Molina (1980) have used the first type of waves as seen in the

5577 OI emission for an estimate of the turbulence diffusion coefficient. The estimate is based on power-spectrum analyses of the observed long-period oscillation in the green-line emission coupled with the theoretical formula for the turbulent diffusion tensor deduced from a statistical theory of turbulence (Weinstock, 1976). The results appear to be very close to those obtained from a linearized monochromatic theory (Hines, 1960) showing that most gravity waves at this height level (~90 km) experience, a small enough frequency spread for a linearized theory to remain valid.

The primary objective of part (3) is to use an extension of the theory of Tuan et al (1979) as well as the dispersion relation developed in part (3) to show that large amplitude primary wave oscillations can producte secondary oscillations with periods of the order of minutes consistent with the observed temporal variations in the 5577A green line as well as the spatial variations observed by Peterson. In the case of the green line, the small period oscillations are usually observed only when the primary wave has rather large amplitudes as mentioned in the introduction. In the case of "ripples" observed by Peterson, whilst a fairly significant primary oscillation with a period of about 2 hours exists on the night of 2-4 Feburary 1973, (Fig. 54), they have not consistently been observed. The possibility therefore remains that some of the "ripples" may either be caused by other mechanisms or may even be themselves primary gravity waves. In this part of the report we shall be only concerned with gravity-wave induced instabilities.

For the analysis of temporal behaviour of the small period oscillations, we use an extension of the theory of Tuan et al (1979) to include the superadiabatic condition (i.e. $\omega_b^2 = \frac{g}{\theta}\frac{d\theta}{dz} < 0$ where ω_b is the Brunt frequency and θ is the temperature potential) for a time duration short compared to the wave period. The latter condition can occur for a small portion of a gravity-wave cycle when its amplitude exceeds some critical value as shown in Fig. 53. The amplitude

of the small period oscillation following a short duration of superadiabatic

condition can, unlike the case of self excitation in Fig. 52, immediately acquire

relatively large values, sometimes comparable to the amplitude of the gravity

wave itself as in Fig. 50. The mathematical formulation for both the solutions

shown in Fig. 52 and Fig. 53 are based on the Semi-Lagrangian formulation of

hydrodynamics. In this formulation, instead of looking for field solutions,

$\psi(\vec{x},t)$ where ψ may be the pressure, the density or the velocity fields, we consider

the trajectory $\vec{x}$ $(\vec{x}_o,t)$ of a fluid particle. Since we may in general neglect

the horizontal motion relative to the vertical owing to the large horizontal

wave length , we may restrict our considerations to the vertical trajectory $z=z(z_o,t)$.

By substituting such a solution into ψ so that $\psi = \psi(z(t),t)$ is a function of

only the time variable we may obtain a fairly simple ordinary equation for $z = z(t)$

if we neglect higher order terms. Thus, by substituting $\psi = \psi(z(t),t)$ into the

hydrodynamic equations and expanding the solution $z(t)$ about $z_G(t) = \overline{X}_o \sin \omega t + z_o$

where z_G is the trajectory of a fluid particle for the linearized gravity waves and ω

is the primary gravity wave frequency, we obtain the following equation for

$z = z(z_o,t)$ to lowest order in $(z - z_G)$.

$$\frac{d^2(z-z_G)}{dt^2} + \eta \frac{d(z - z_G)}{dt} + \omega_H^2(t)(z - z_G) = f(z_G,t) \tag{21}$$

In equation (21)

$z_G = \overline{X}_o \sin (t - t_o) + z_o$ is the vertical displacement of the primary
gravity wave.

η = a coefficient which will depend on the turbulence viscosity in
some complicated way but will be used primarily as a parameter
for this report.

- 29 -

$$\omega_H^2(t) = -g\left[\frac{1}{\rho_B}\frac{\partial\rho_B}{\partial z} + \frac{g}{2}\right]$$

$$\sim \omega_B^2\{[1 + k_z\overline{X} \sin[\omega(t - t_o) - k_z(z_G - z_o)]]\}$$

$f(z_G,t)$ = forcing functions and is usually small.

We see immediately that the superadiabatic condition occurs if $k_z\overline{X}_o > 1$ when ω_H^2 turns negative for a portion of the gravity-wave cycle. During this period, turbulence is generated, causing the more violent small period oscillations to follow, Fig. 53.

If the short-period oscillations should give rise to secondary waves the spatial variations of such waves may be analyzed by the dispersion relation discussed in part (3). One possible mechanism for producing such waves is the growth of a primary gravity wave with height until instability occurs at some regions in the mesosphere. For gravity waves guided from a relatively distant source, the wave will be stationary along the vertical direction and instability of the type just discussed can occur over the shaded regions shown in Fig. 54. Such instability can occur periodically over the periods of the primary gravity wave, provided it maintains its strength. If the primary gravity wave should be a travelling wave, then the region of instability and turbulence would propagate along with the gravity wave.

Summary and Conclusion

In this section we summarize the basic physics that are pertinent to spatial
and temporal infrared variance produced by atmospheric gravity waves. There
are in general two types of gravity waves. The type which produce the large-
scale T.I.D.'s are characterized by (see Thome, (1968);

(i)   Energy concentrated at high altitudes with little wave amplitude
      below 110 km.

(ii) High horizontal phase velocity (in excess of 400 m sec^{-1}).

(iii) Source also located at high altitudes, usually from polar
      magnetospheric substorms.

(iv) Usually travel along longitudes and exhibit little inclination
      to go past the equator.

The type which produce the medium-scale T.I.D.'s are characterized by (Thome,
(1968), Battaner & Molina (1980), Hines, (1960)).

(i)   Energy mostly concentrated at low altitudes but can spread up to high
      altitudes

(ii) Low horizontal phase velocities (less than 400 m sec^{-1}).

(iii) Source is usually at low altitudes and are often due to
      meteorological conditions

(iv) Do not travel in any preferred longitudinal or latitudinal
      direction.

Gravity waves should also be divided into two categories:

(i)   Those with small enough amplitudes so that the waves may be accurately
considered as purely linear waves. These gravity waves constitute a majority
of the waves which are far from their sources.

(ii) Waves with large enough amplitudes where non-linear effects,

- 31 -

coupling to background Brunt-Vaisala Oscillation, frequency spreading, induced instability and turbulence become important. For the lower altitude waves (medium-scale T.I.D.'s), where many of the sources occur near the ground level, the increase in velocity amplitude with height can often cause the Richardson's number to fall below critical values, thus producing instability and turbulence. The growth of wave amplitudes will eventually be damped out by viscosity, heat conduction and ion drag at higher altitudes. The wave saturation usually occurs above mesospheric altitudes which leave the mesospheric regions with the largest wave amplitude and hence the maximum degree of turbulence.

With this summary of gravity-wave characteristics we see immediately that since most of the more intense infrared emissions come from lower altitudes (below 100 km), only the type of gravity waves which produce the medium-scale T.I.D.'s can have an important effect. These waves have been investigated by Battaner & Molina (1980) and Hines (1960). The results may be summarized as follows:

(i)   Gravity Waves vary in frequency and periods in the range between 1 and 7 hours with the most often occurring periods between 2 and 3.5 hours.

(ii)   Seasonal variations show a Winter and Summer maxima.

(iii)   Horizontal phase velocities vary between 30 and 140 m sec^{-1} with a median of between 80-100 m sec^{-1}.

Based on the above summary we have chosen for this report gravity waves with periods of two hours and horizontal phase velocities ranging from 60 m sec^{-1} to 129 m sec^{-1} all of which correspond to the most frequently occurring low-altitude gravity waves.

The major portion of this report deals with the effect of linear gravity waves on the spatial and temporal structure of minor atmospheric constituents which produce infrared emissions as well as the infrared emission profiles. Since chemical equilibrium has been universally assumed, it is the effect of gravity

waves on the initial atmospheric components which produce the excited vibrational
states that primarily determine the spatial and temporal behavior of the infrared
emissions which occur as a result of these vibrational states returning to the
ground states.

We have found two possibilities which determine the basic features of the
spatial structures of the infrared emission profile:

(1) If the excited vibrational states of the infrared emitter occur locally
as a direct result of chemical reaction such as OH emission which occur mainly
due to the exchange reaction of hydrogen with ozone leaving the hydroxyl molecule
in an excited vibrational state (Myrabø et al (1983)), the spatial infrared profile would
show wave-like structures just as strongly as the number density profiles of
hydrogen and ozone.

(2) If the excited vibrational states are not produced locally such as
the case for chemical reactions but are mainly produced through absorptions of
infrared radiation from extended sources such as either the earth considered
as a blackbody radiation source or other atmospheric molecules which extend over
the entire atmosphere, the structures would be modified through integrations
over the extended sources. The infrared emitters such as CO_2, NO, O and H_2O
considered in this report largely belong to this class. For such emitters the
infared radiation profile would be less sharply structured than the individual
number density profiles.

The temporal behaviour would in general be far less strongly influenced
by the nature of the source and the excitation mechanism. Since part of the
present report is in collaboration with Visidyne which is at present working
on the temporal radiation profiles, we will postpone discussion of this to a
later report.

The general characteristics of wave-induced infrared spatial structures

- 33 -

must show similar characteristics as wave structures. Thus, we would expect:

(1) Spatial structures relative to background should increase with altitude, since such structures depend generally on gravity-wave velocity amplitudes which also increase with altitude. Irregular structures as seen in the CO_2 radiance profile by Sharma and Nadile (1980) are unlikely to be due to a gravity wave because the structure occurring between 95 km and 110 km does not repeat itself with greater severity at higher altitudes. However, if a gravity wave has high horizontal phase velocity (and hence long vertical wave length) it is possble that a single structure will appear at say 110 km but will only reappear at sufficiently high altitudes that damping would serve to erase it. In fact, precisely such a structure appears near 110 km in the CO_2 profile for a horizontal phase velocity of 129 m sec^{-1} in Fig. 8. For gravity waves with shorter vertical wave length (Fig. 13) and lower horizontal phase velocity (60 m sec^{-1}) we see that the structure increases in amplitude further up. However, the damping does not really become excessive until several hundred kilometers and we hence regard the possibility that the structure seen by Sharma and Nadile as being caused by a gravity wave as small.

(2) If the minor atmospheric constituent has a layered structure, in other words it is not in hydrostatic equilibrium, the oscillation of the constitutent should be 180° out of phase with the gravity wave where its ambient concentration gradient is positive, opposite to the major atmospheric constituents (bottom side of layer) and in phase with the gravity wave where its ambient concentration gradient is negative, the same as the major constituents (top-side layer). This result has been shown by Hatfield et al (1981) and has a long history. The corresponding infrared emission should show a similar phase change, especially if the excited vibrational states are produced locally from a chemical reaction.

(3) We have investigated the infrared variance with:

- 34 -

(a) Free gravity waves with vertical wave length short compared with background atmospheric structure.

(b) Guided gravity waves (Lamb Mode) with vertical wave length long compared with background atmospheric structure e.g. Fig. 2) We have found that:

(i) Gravity waves with short vertical wave length can produce both spatial and temporal variations in the number density profile and hence in the radiance profile.

(ii) Gravity wave with long vertical wave length such as the guided Lamb mode can only produce temporal variations in the number density and also the infrared emission profiles. For this case the radiance profile should show no extraneous spatial structures (Fig. 2 and 3) but only periodic variations as a function of time in the zenith columnar intensity in infrared emissions.

The remainder of the report deals with gravity waves with large enough amplitudes to produce instability in the mesospheric regions. We have found that for $k_z \underline{\bar{X}} > 1$ (where k_z is vertical wave vector and $\bar{X}$ is the vertical displacement amplitude) which typically corresponds to $\bar{X} \sim 1.5$ km in the mesospheric region instability can occur and give   rise to secondary oscillations with periods of the order of Brunt period. In very rough calculations we found that $\bar{X} = 1.5$ km in displacement would require a density, pressure or temperature variation of 20%. All the experimental evidence in airglow, (Okuda (1975)), P.R.D. (Manson et al (1981)) and temperature waves (Myrabo et al (1983)) seem to suggest that such large variations will produce secondary oscillations.

The spatial analyses of these secondary oscillations at an altitude close to the mesopause and with periods close to the Brunt period cannot be done with

- 35 -

the Hines' dispersion relation. A new dispersion relation which remains valid in an inhomogeneous medium has been developed for this report. The results show that the Hines' dispersion relation holds well for all but the frequencies close to either the Brunt or the acoustic cut-off frequencies. Close to such frequencies the vertical wave vector, k_z, tends to zero near the turning point where heavy wave reflection takes place and the Hines' relation derived for a homogeneous isothermal medium can no longer be valid. It is also precisely within the range of these frequencies that all the observed secondary oscillations appear to lie. Hence, the generalized dispersion relation has been developed to analyze secondary waves arising from these secondary oscillations.

The detailed technique required to analyze the optical emissions data, the temperature wave data as well as to extract from these data the means to determine atmospheric parameters such as turbulence viscosity and energy dissipation rate will be relegated to a future report. Experimental procedures for measuring long term infrared optical emissions in order to obtain morphology on long-term mesospheric disturbance will also be part of this future program.

Bibliography

(1) Andrews, M.K., Wave-like irregularities in the mid-latitude 6300 $\overset{o}{A}$ airglow, Planet. Space Sci. 24, 521-527 (1976).

(2) Armstrong, E.B., The influence of a gravity wave on the airglow hydroxyl rotational temperature at night, J. Atmos. Terr. Phys. 37, 1585-1591 (1975).

(3) Barbier, D., Observation photometrique d'une perturbation de la haute atmosphere, Astrophys. Norv. 9, 55-59, (1964).

(4) Barbier, D., Deux phenomenes particulars presentee par le raie rouge de la lumiere du ciel nocturne Ann. Geophys. 21, 228-234, (1965).

(5) Battaner, E. and A. Molina, Turbopause internal gravity waves, 557.7 nm airglow and eddy diffusion coefficient, J. Geophys. Res. 85, 6803-6810, (1980).

(6) Battaner, E., A. Molina and J.M. Quintane, Proc. of the 5th European Meeting of upper atmsopheric studies by optical methods, Granada, (1977).

(7) Chow, W. and T.F. Tuan, Assessment on $CO_2(\nu_2)$ radiance profile, (1980).

(8) Dachs, J. Die Helligkeiten des nachtlichen Luftleuchtens wahrend des Sonnenflecken-minimums nach Messungen in Südwestafrika Beitr. Phys. Atmos. 41, 184-215, (1968).

(9) Dyson, P.L. and P.A. Hopgood, Fluctuations in mid-latitude 6300 $\overset{o}{A}$ airglow and their relationship to F-region irregularities, Planet. Space Sci. 26, 161-169, (1978).

(10) Francis, S.H., Global propagation of atmospheric gravity waves: A review, J. Atmos. Terr. Phys. 37, 1011-1054 (1975).

(11) Hatfield, R., T.F. Tuan and S.M. Silverman, On the effects of atmospheric gravity waves on profiles of H, O_3 and OH emission, J. Geophys. Res., 86, 2429-2437, (1981).

(12) Hines, C.O., Internal atmospheric gravity waves at ionospheric heights, Can. J. Phys., 38, 1441-1481, (1960).

(13) Hines, C.O., The upper atmosphere in Motion, Geophys. Mono., 18, A.G.U., Washington, D.C., (1974).

(14) Hodges, R.R., Generation of turbulence in the upper atmosphere by internal gravity waves, J. Geophys. Res., 72, 3455-3458, (1967).

(15) Kieffaber, L.M., Structure and fluctuation of the OH airglow, Thesis Dept. of Physics and Astronomy, Univ. of N.M., (1973).

(16) Krassovsky, V.I., Nature of the intensity variations of the terrestrial atmosphere emission, Mem. Soc. R. Sci. Liege 18, 58-67, (1957).

(17) Krassovsky, V.I., Infrasonic variation of OH emission in the upper atmmosphere, Ann. Geophys. 28, 739-746, (1972).

(18) Krassovsky, V.I. and M.V. Shagaev, Optical method of recording acoustic gravity waves in the upper atmosphere, J. Atmos. Terr. Phys. 36, 373-375, (1974).

(19) Krassovsky, V.I. and M.V. Shagaev, On the nature of internal gravity waves observed from hydroxyl emission, Planet. Space Sci., 25, 200-201, (1977).

(20) Krassovsky, V.I., B.P. Potapov, A.I. Seminov, M.V. Shagaev, N.N. Shepov, V.G. Sobolev and T.I. Toroshuledze, Internal gravity waves near the mesopause and the hydroxyl emission, Ann. Geophys. 33, 347-356, (1977).

(21) Manson, A.H. and C.E. Meek, Gravity waves of short period (5-90 min) in the lower thermosphere at 52° N (Sackatoon, Canada), J. Atmos. Terr. Phys., 42, 103-113, (1980).

(22) Manson, A.H., C.E. Meek and J.B. Gregory, Gravity waves of short period (5-90 min), in the lower thermosphere at 52°N (Saskatoon, Canada); 1978/1979, J. Atmos. Terr. Phys., 43, 35-44 (1981).

(23) Midgley, J.E. and H.B. Liemohn, Gravity waves in a realistic atmosphere, J. Geophys. Res., 3729-3748, (1966).

(24) Moreels, G. and M. Herse, Photographic evidence of waves around the 85 km level, Planet. Space Sci., 25, 265-271, (1977).

(25) Myrabo, H.K., C.S. Deehr and G.G. Sivjee, Large amplitude night glow OH (8-3) band intensity and rotational temperatures variations during a 24 hour period at 78°N, preprint (1983).

(26) Okuda, M., A study of excitation process in nightglow, Sci. Rep. Tokuho Univ. Ser. 5, 14, 9-26, (1962).

(27) Okuda, M., Private Communication (1975).

(28) Papadopoulos, D., A.W. Peterson, T.F. Tuan and R.M. Nadile, A generalization of the Hines' dispersion relation to an inhomogeneous atmosphere, Preprint (1982).

(29) Peterson, A.W., Airglow events visible to the naked eye, Appl. Opt. 18, 3390-3393, (1979).

(30) Peterson, A.W. and L.M. Kieffaber, Infrared Photography of OH airglow structures, Nature, 242, 321, (1973).

(31) Peterson, A.W. and L.M. Kieffaber, Photography and photometry of the near infrared OH airglow, Nature, 257, 649, (1975).

(32) Pittaway, M.L.V. and C.O. Hines, The viscous damping of atmospheric gravity waves, Can. J. Phys., 41, 1935-1948, (1963).

(33) Porter, H.S., S.M. Silverman and T.F. Tuan, On the behaviour of airglow under the influence of gravity waves, J. Geophys. Res. 79, 3827-3833, (1974).

(34) Roper, R.G., The upper atmosphere and Magnetosphere, National Academy of Sciences, Washington, D.C. (1977).

(35) Sharma, R.D. and R.M. Nadile, Carbon dioxide (ν_2) radiance results using a new non-equilibrium model, paper presented at the SPIRE Meeting Chemistry Conference at AIAA 19th Aerospace Sciences Meeting, St. Louis, MO AIAA-81-0426, (1981).

(36) Silverman, S.M., Universal fluctuations of 5577 $\overset{o}{A}$ OI emission intensity on October 28-29, 1961, Nature, 195, 481-482, (1962).

(37) Thome, G.D., Long-period waves generated in the polar ionosphere during the onset of magnetic storms, J. Geophys. Res. 73, 6319-6336, (1968).

(38) Tuan, T.F., Research in gravity waves and airglow phenomena, Rep. AFGL-TR-76-0296, Air Force Geophys. Lab., Bedford, Mass., (1976). AD A040414

(39) Tuan, T.F., R. Hedinger, S.M. Silverman and M. Okuda, On gravity wave induced Brunt-Vaisala Oscillations, J. Geophys. Res., 84, 393, (1979).

(40) Tuan, T.F. and D. Tadic, A dispersion formula for analyzing "Modal interference" among guided and free gravity wave modes and other phenomena in a realistic atmosphere, J. Geophys. Res. 87, 1648-1668, (1982).

(41) Volland, H., Full wave calculations of gravity wave propagations through the thermosphere, J. Geophys. Res., 74, 1786-1795, (1969).

(42) Weill, G. and J. Christophe-Glaume, L'excitation du doublet interdit $^4S-^2D$ de l'azote observee dans la luminescence nocturne an cours d'une perturbation ionospherique itinerante, C.R. Acad. Sci., 264, 1286-1289, (1967).

(43) Weinstock, J., Nonlinear theory of acoustic gravity waves, 1, saturation and enhanced diffusion, J. Geophys. Res. 81, 633-652, (1976).

(44) Yeh, K.C. and C.H. Liu, Acoustic gravity waves in the upper atmosphere, Rev. Geophys. Space Phys., 12, 193-216, (1974).

(45) Yu L., T.F. Tuan and H. Tai, On "potential" well treatment for atmospheric gravity waves, J. Geophys. Res. 85, 1297-1305, (1980).

(46) Zimmerman, S.P. and E.A. Murphy, Dynamical and chemical coupling of the neutral and ionized atmosphere, D. Reidal, Hingham, Mass., (1977).

Data Set F (T_{ex}=1555.7°K)
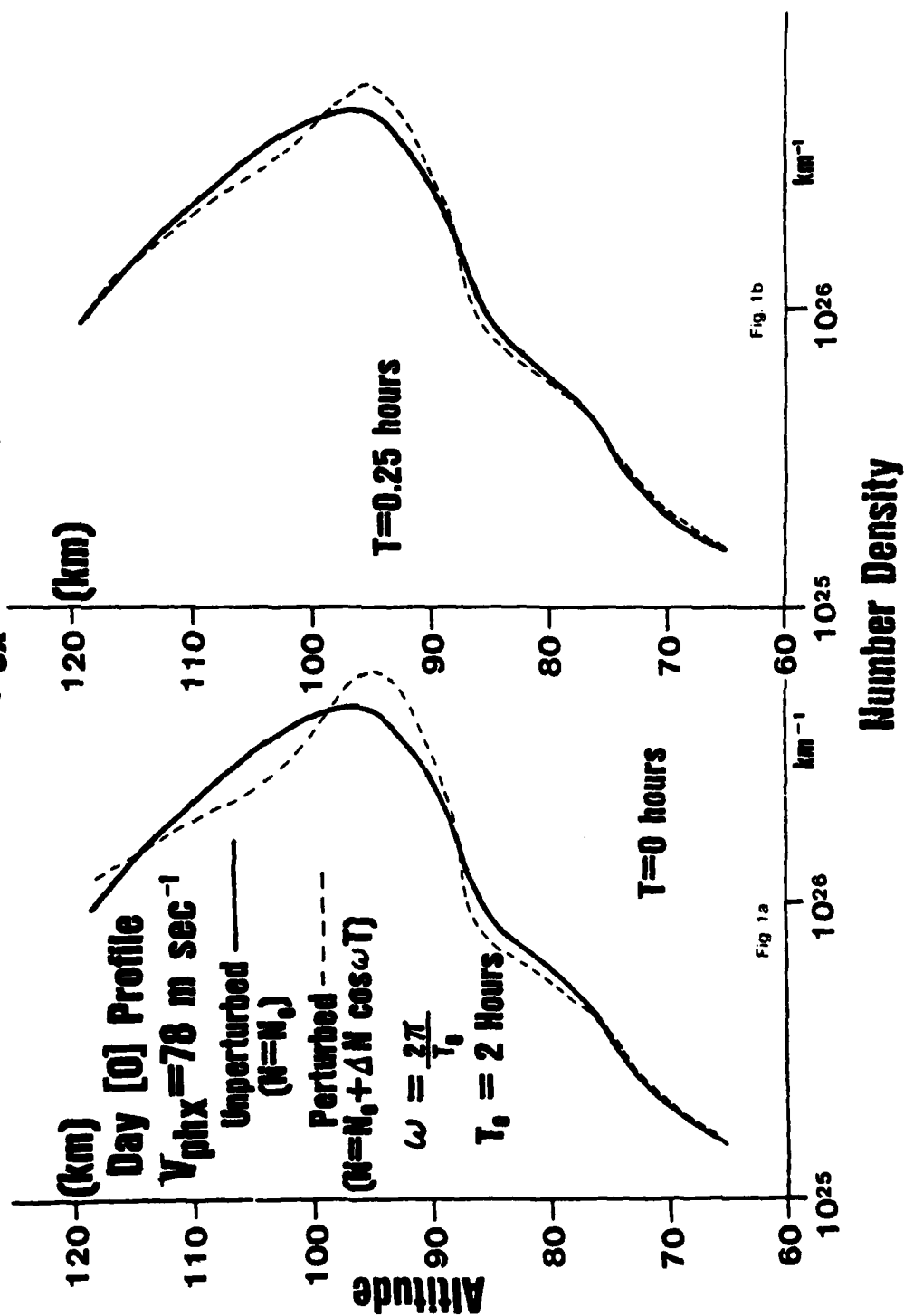
Day [0] Profile
V_{phx}=78 m sec^{-1}

Unperturbed ——— ($N=N_0$)

Perturbed - - - - ($N=N_0+\Delta N \cos\omega T$)

$\omega = \frac{2\pi}{T_0}$

T_0 = 2 Hours

T=0 hours

Fig 1a

T=0.25 hours

Fig. 1b

Altitude

Number Density

Data Set F (T_{ex}=1555.7°K)

Day [0] Profile
V_{phx}=78 m sec^{-1}

Unperturbed ———
($N=N_o$)

Perturbed – – –
($N=N_o+\Delta N \cos\omega T$)

T_s = 2 Hours

T=1.0 hours

T=0.75 hours

Fig. 1d

Fig. 1c

Number Density

- 42 -

Data Set F (T_{ex}=1555.7°K)

Day [0] Profile (V_{phx}=301.5m sec^{-1}) (Partially Guided Lamb Mode)

—— Unperturbed
($N=N_0$)

——— Perturbed
($N=N_0+\Delta N \cos\omega T$)

$\omega = \dfrac{2\pi}{T_0}$

T_0 = 2 Hours

Number Density

Fig. 2

Altitude (km)

- 43 -
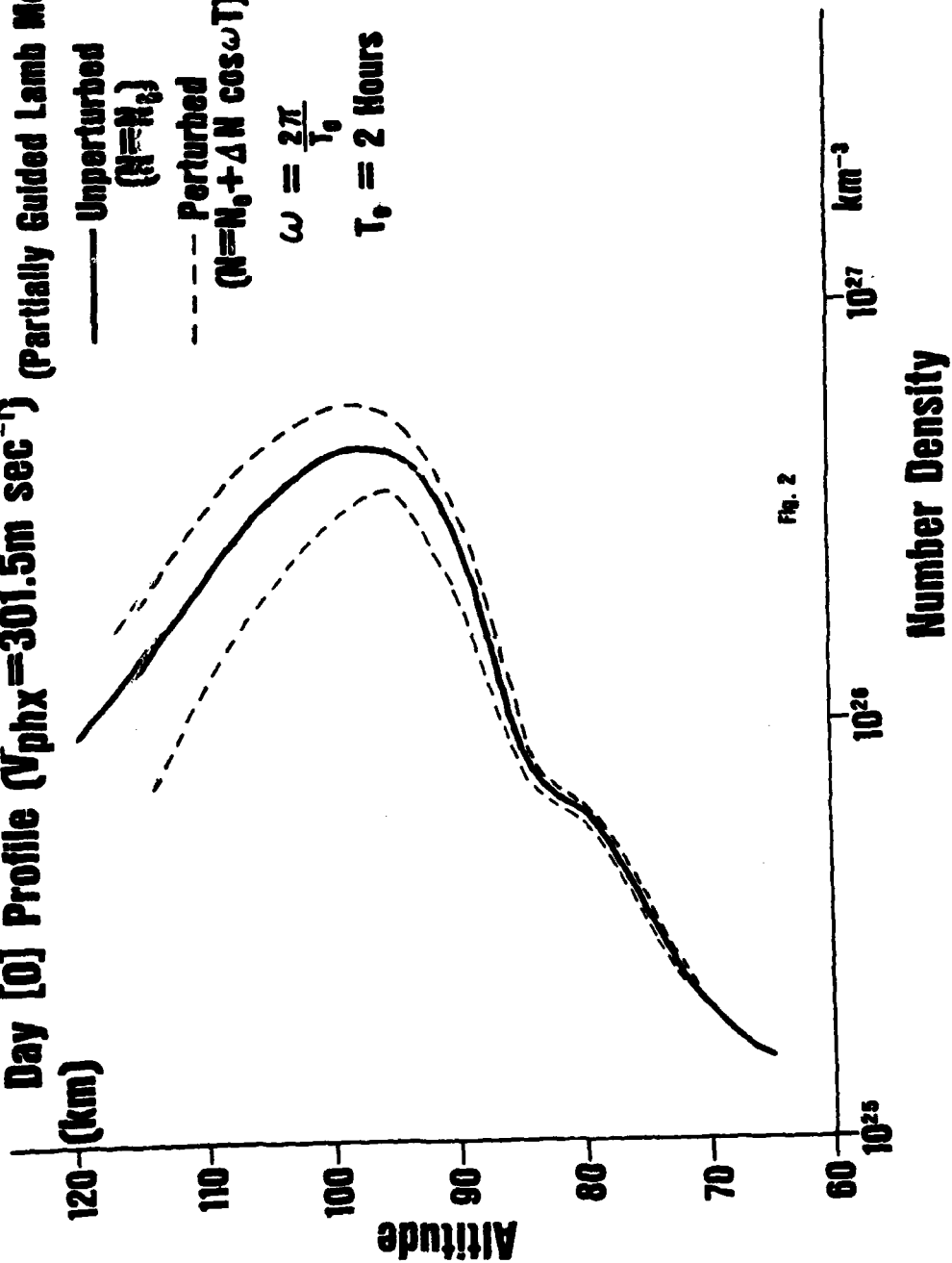
Data Set F (T_{ex}=1555.7°K)

Day [NO] Profile (V_{phx}=301.5m sec^{-1}) (Partially Guided Lamb Mode)

Unperturbed
($N=N_0$)

Perturbed
($N=N_0+\Delta N \cos \omega T$)

$\omega = \dfrac{2\pi}{T_0}$

$T_0 = 2$ Hours

T=1.0 hours

T=0 hours

Altitude (km)

Number Density   km^{-3}

Fig. 3

- 44 -

Data Set F (T_{ex}=1555.7°K)
Day [0] Profile
—— Unperturbed
--- Perturbed

V_{phx}=129 m sec^{-1}
(A=60)

Fig. 4

Number Density

Altitude

- 45 -

Data Set F ($T_{ex} = 1555.7°K$)

Night [D] Profile

——— Unperturbed

– – – Perturbed

$V_{phx} = 129\ m\ sec^{-1}$

$(\Lambda = 60)$

Altitude (km)

Number Density km^{-3}

Fig. 5

- 46 -

Data Set F (T_{ex}=1555.7°K)

Day [NO] Profile
——— Unperturbed
----- Perturbed

V_{phx}=129 m sec^{-1}
(A=60)

Altitude (km)

Number Density   km^{-3}

Fig. 8

Fig. 7

Data Set F (Tex

Night [NO] Profile
——— Unperturbed
– – – Perturbed

$V_{phx} = 129$ m sec^{-1}
(A = 60)

Number Density

km^{-3}

10^{21} 10^{22} 10^{23}

Altitude (km)

120 110 100 90 80 70 60

Data Set F (T_{ex}=1555.7°K)
[CO_2] Profile
—— Unperturbed
----- Perturbed
V_{phx}=129m sec^{-1}
(A=60)

Fig. 8

Number Density

Altitude

Data Set A (T_{ex}=626.5°K)
Day [O] Profile
—— Unperturbed
--- Perturbed

V_{phx}=60 m sec^{-1}
(A=278)

Fig. 9

Number Density

Altitude

120 (km)
110
100
90
80
70
60

10^{25} 10^{26} 10^{27} km^{-3}

Data Set A (T_{ex}=626.5°K)
Night [O] Profile
—— Unperturbed
--- Perturbed
V_{phx}= 60 m sec^{-1}
(Λ=278)

Altitude (km)

Number Density km^{-3}

Fig. 10

- 51 -

Data Set A (Tex=626.5°K)

Day [NO] Profile
— Unperturbed
- - - - Perturbed

$V_{phx} = 60 \text{ m sec}^{-1}$
(A=278)

Altitude (km)
120
110
100
90
80
70
60

Number Density   km⁻³
10²¹   10²²   10²³

Fig. 11

Night [NO] Profile
—— Unperturbed
----- Perturbed

Data Set A (T_{ex}=626.5°K)

V_{phx}= 60 m sec^{-1}
(A=278)

Fig. 12

Altitude (km)

Number Density   km^{-3}

Data Set A ($T_{ex} = 626.5°K$)

$[CO_2]$ Profile
——— Unperturbed
- - - Perturbed

$V_{phx} = 60$ m sec^{-1}
($A = 278$)

Fig. 13

Number Density

Altitude

(km)

km^{-3}

- 54 -
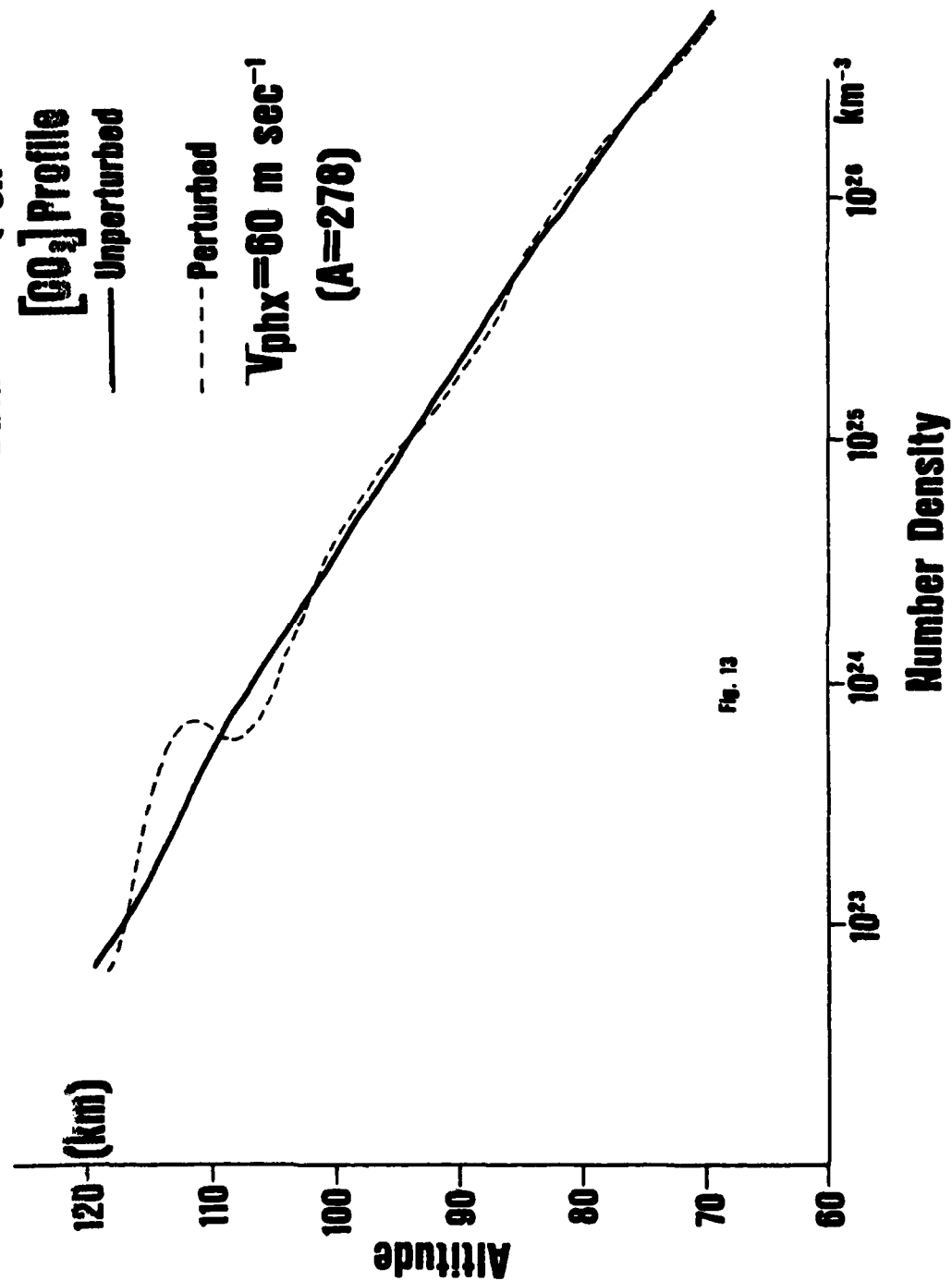
Data Set C (T_{ex}=1081.2°K)
Day [0] Profile
——— Unperturbed
- - - Perturbed

V_{phx}=78 m sec^{-1}
(A=163)

Fig. 14

Number Density

km^{-3}

Altitude

(km)

- 55 -

Data Set C (T_{ex}=1081.2°K)

Night [O] Profile
— Unperturbed
--- Perturbed

V_{phx}=78 m sec^{-1}
(A=163)

Fig. 15

Altitude (km)

Number Density   km^{-3}

Fig. 18

Fig. 17

Number Density

km^{-3}

10^{23} 10^{22} 10^{21}

Altitude (km)

120 110 100 90 80 70 60

Data Set C (T_{ex} = 1081.2°K)

Night [NO] Profile

——— Unperturbed
- - - - - Perturbed

V_{phx} = 60 m sec^{-1}
(A = 278)

- 58 -
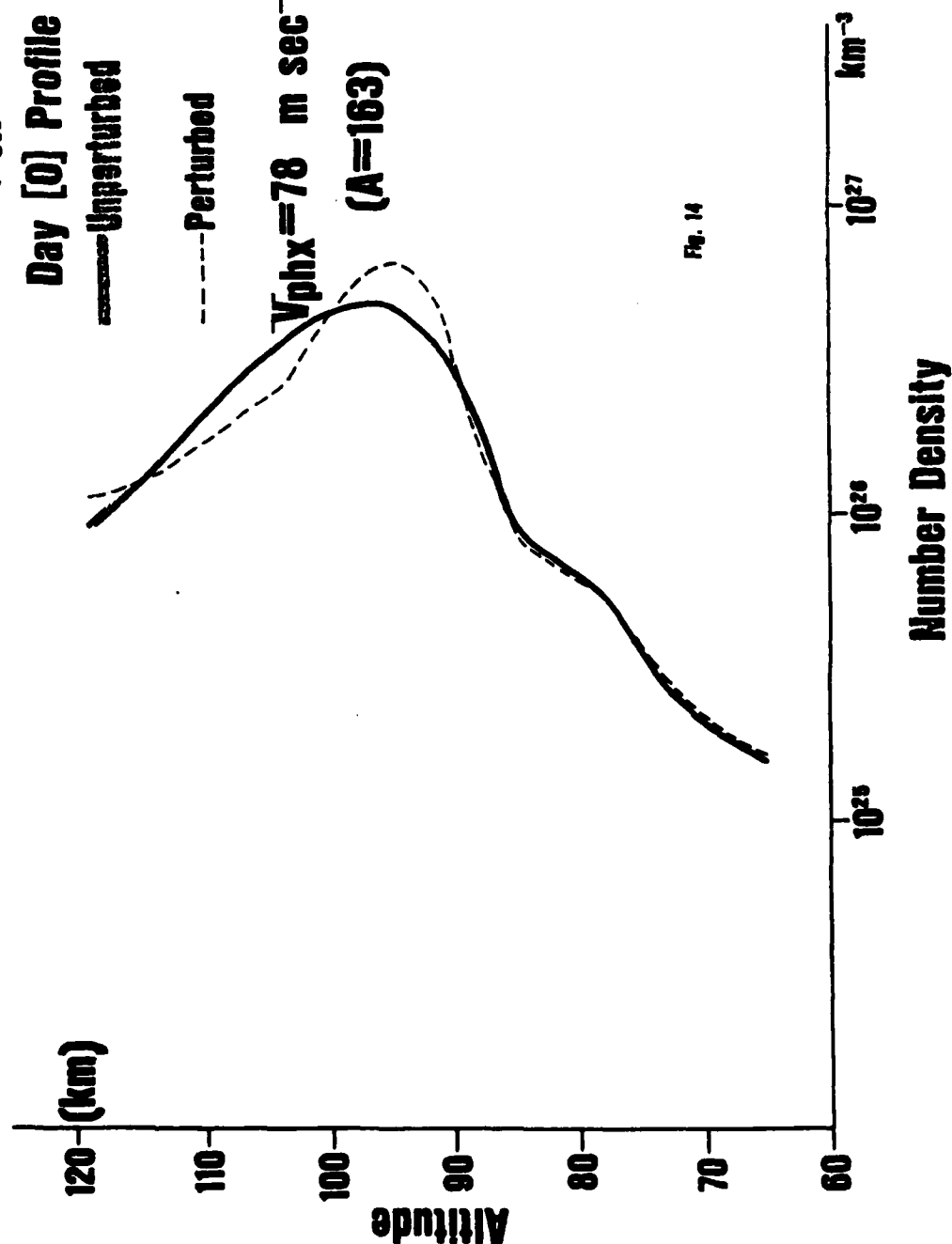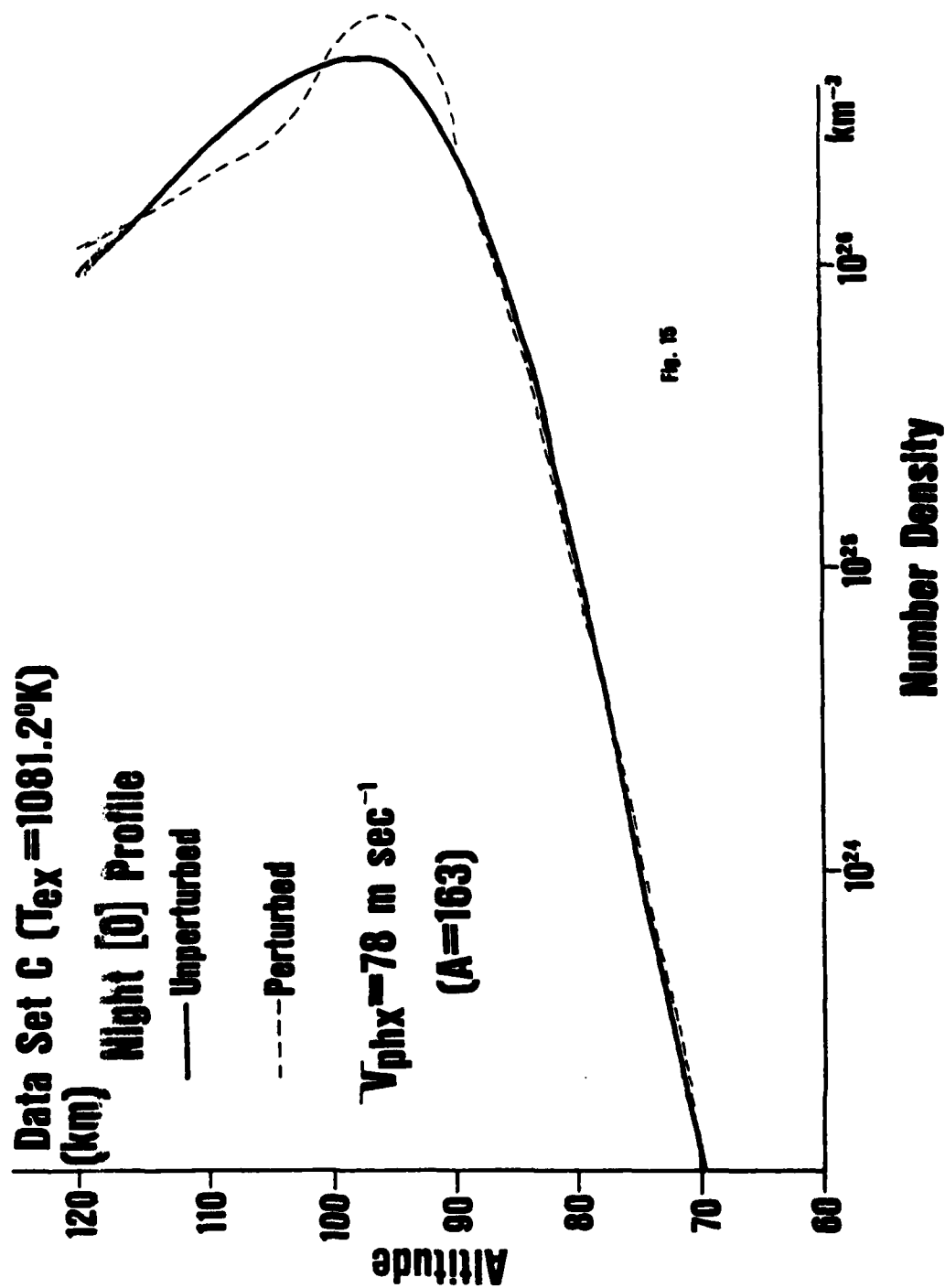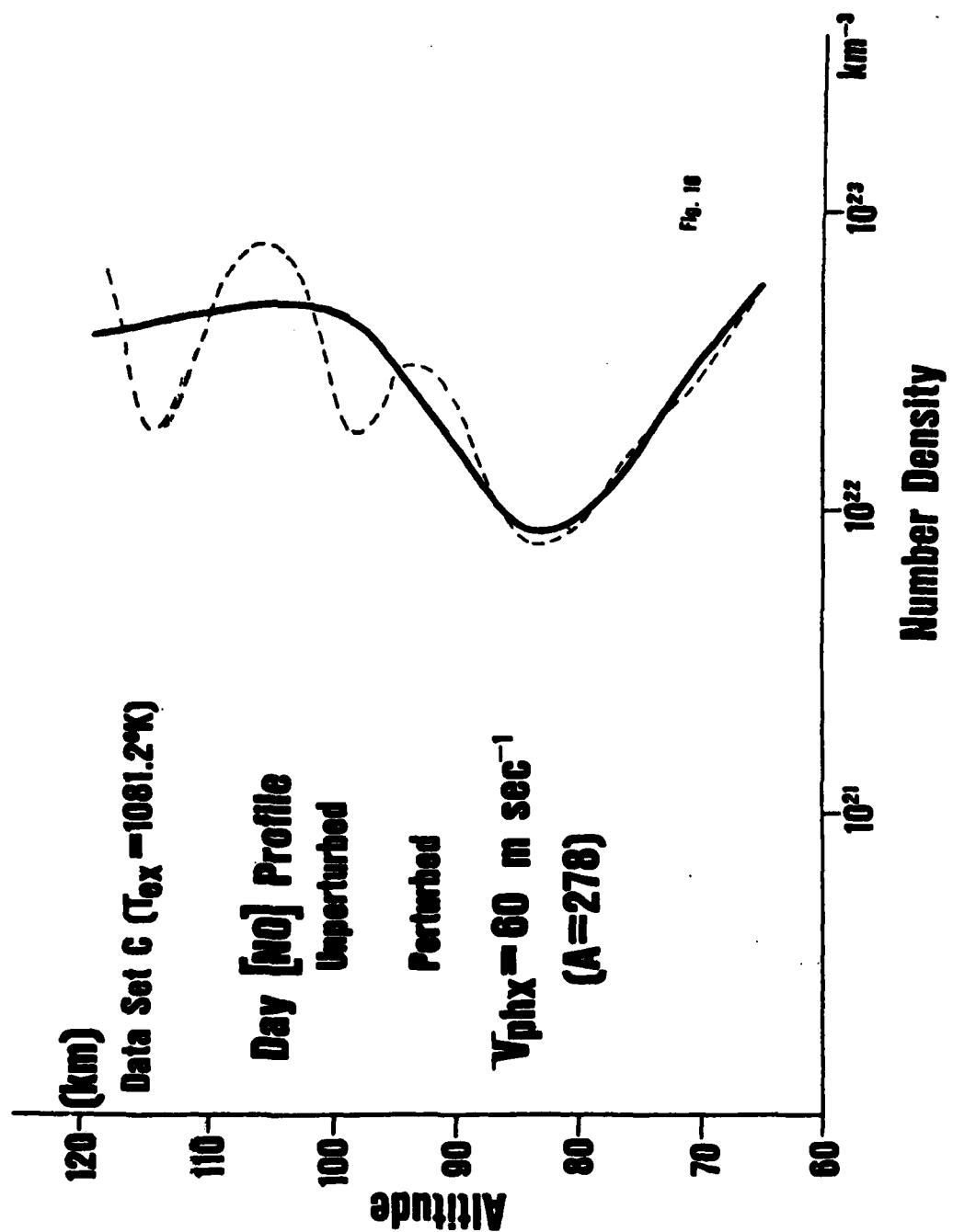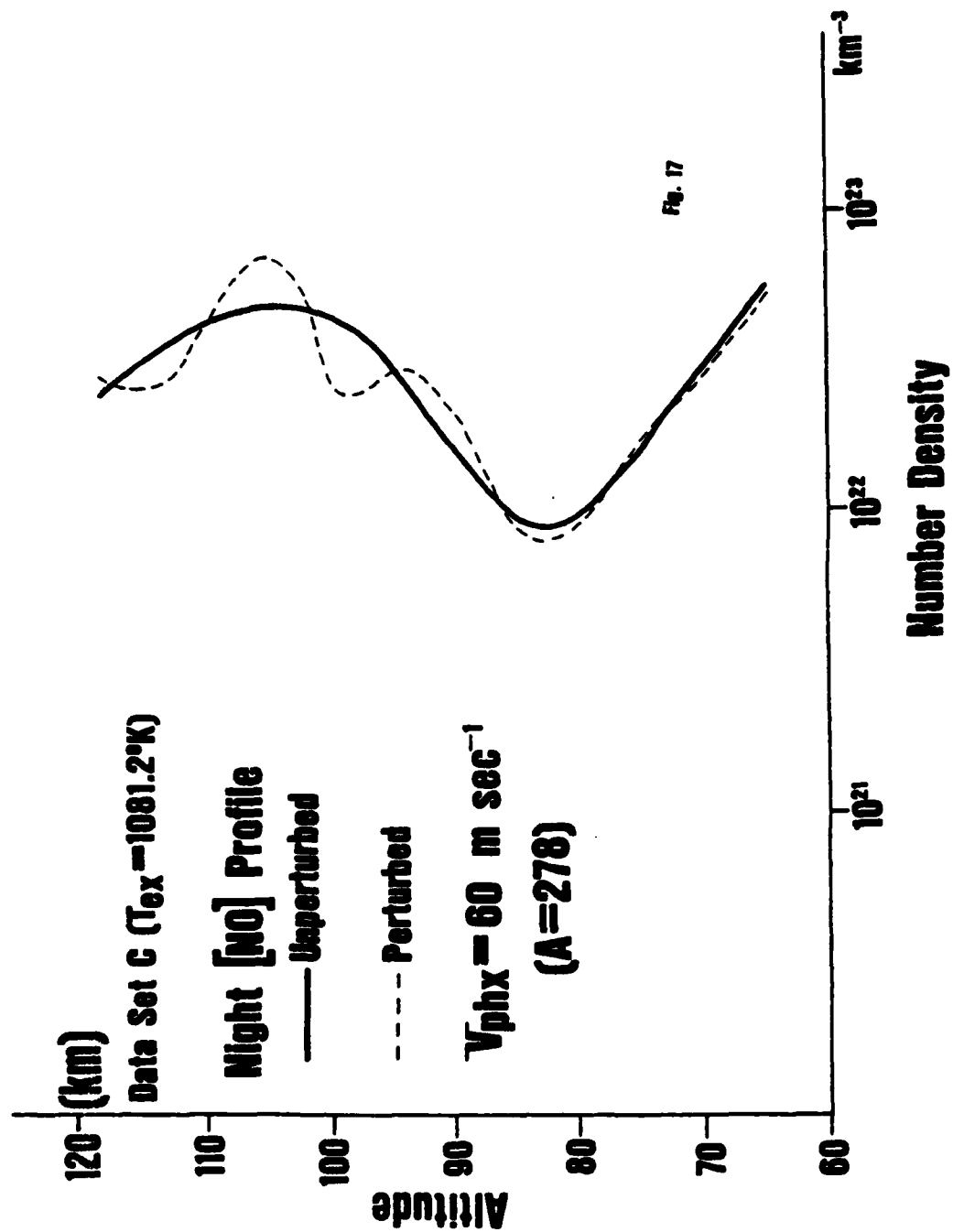
Data Set C (T_{ex}=1018.2°K)

[CO_2] Profile
Unperturbed

Perturbed

V_{phx}=60 m sec^{-1}

(A=278)

Number Density   km^{-3}

Altitude (km)

Fig. 18

- 59 -

Data Set F (T_{ex}=1555.7^{0}K)
Day [0] Profile
— Unperturbed
--- Perturbed

V_{phx}=78 m sec^{-1}
(A=163)

Number Density

Altitude [km]

km^{-3}

Fig. 18

Fig. 20

Data Set F (T_{ex}=1555.7°K)

Night [0] Profile

—— Unperturbed

---- Perturbed

V_{phx}= 78 m sec^{-1}

(λ=183)

Altitude (km)

Number Density km^{-3}

Data Set F (T_{ex}=1555.7°K)

Day [NO] Profile
——— Unperturbed
- - - - Perturbed

V_{phx}=60 m sec^{-1}
(A=278)

Altitude (km)

Number Density km^{-3}

Fig. 21

- 62 -

Data Set F (T_{8x} =1555.7°K)

Night [NO] Profile
—— Unperturbed
----- Perturbed

V_{phx} = 60 m sec^{-1}
(A=278)

Fig. 22

Altitude (km)

Number Density km^{-3}

Data Set F (T_{ex}=1555.7°K)
[CO_2] Profile
——— Unperturbed
- - - - Perturbed
V_{phx}=60 m sec^{-1}
(A=278)

Fig. 23

Number Density

Altitude

Data Set G ($T_{ex}=1829.4°K$)
Day [O] Profile
—— Unperturbed
----- Perturbed
$V_{phx}=78$ m sec^{-1}
(A=163)

Fig. 24

Number Density

Altitude (km)

120 110 100 90 80 70 60

10^{25} 10^{26} 10^{27} km^{-3}

- 65 -

Data Set G (T_{ex}=1829.4°K)

(km) Night [0] Profile

Unperturbed

Perturbed

V_{phx}=78 m sec⁻¹)

(A=163)

Fig. 25

Number Density   km⁻³

Altitude

- 66 -

Fig. 28

Data Set 6 (T$_{ex}$=1828.4^{0}K)

Day [NO] Profile
——— Unperturbed
- - - - Perturbed

V$_{phx}$= 60 m sec^{-1}
(Λ=278)

Altitude (km)

Number Density km^{-3}

- 67 -

Fig. 27

Data Set G (T_{ex} = 1829.4°K)

Night [NO] Profile
—— Unperturbed
----- Perturbed

V_{phx} = 60 m sec^{-1}
(A = 278)

Number Density   km^{-3}

Altitude (km)

Data Set G (T_{ex}=1829.4°K)
[CO_2] Profile
—— Unperturbed
---- Perturbed
V_{phx}=60 m sec^{-1}
(A=278)

Fig. 26

Number Density

Altitude

120 (km)
110
100
90
80
70
60

10^{23} 10^{24} 10^{25} 10^{26} km^{-3}

Data Set H (Tex=2176.8°K)
Day [0] Profile
Unperturbed ———
Perturbed - - - -

$V_{phx} = 78 \text{ m sec}^{-1}$
(A=163)

Fig. 28

Number Density

Altitude

(km)

120
110
100
90
80
70
60

10^{25} 10^{26} 10^{27} km^{-3}

- 70 -

Data Set H ($T_{ex} = 2176.8°K$)

Night [O] Profile

—— Unperturbed

- - - - Perturbed

$V_{phx} = 78$ m sec^{-1}

($A = 163$)

Altitude (km)

Number Density

km^{-3}

Fig. 30

- 71 -

Data Set H (T_{ex} = 2176.8°K)

Day [NO] Profile
—— Unperturbed
----- Perturbed

V_{phx} = 60 m sec^{-1}
(A=278)

Fig. 31

Altitude (km)

Number Density km^{-3}

- 72 -

Fig. 32

Night [NO] Profile
——— Unperturbed
---- Perturbed

Data Set H (T_{ex}=2176.8°K)

V_{phx} = 60 m sec^{-1}
(A=278)

Altitude (km)

Number Density km^{-3}

Data Set H (T_{ex} =2176.8°K)
$[CO_2]$ Profile
—— Unperturbed
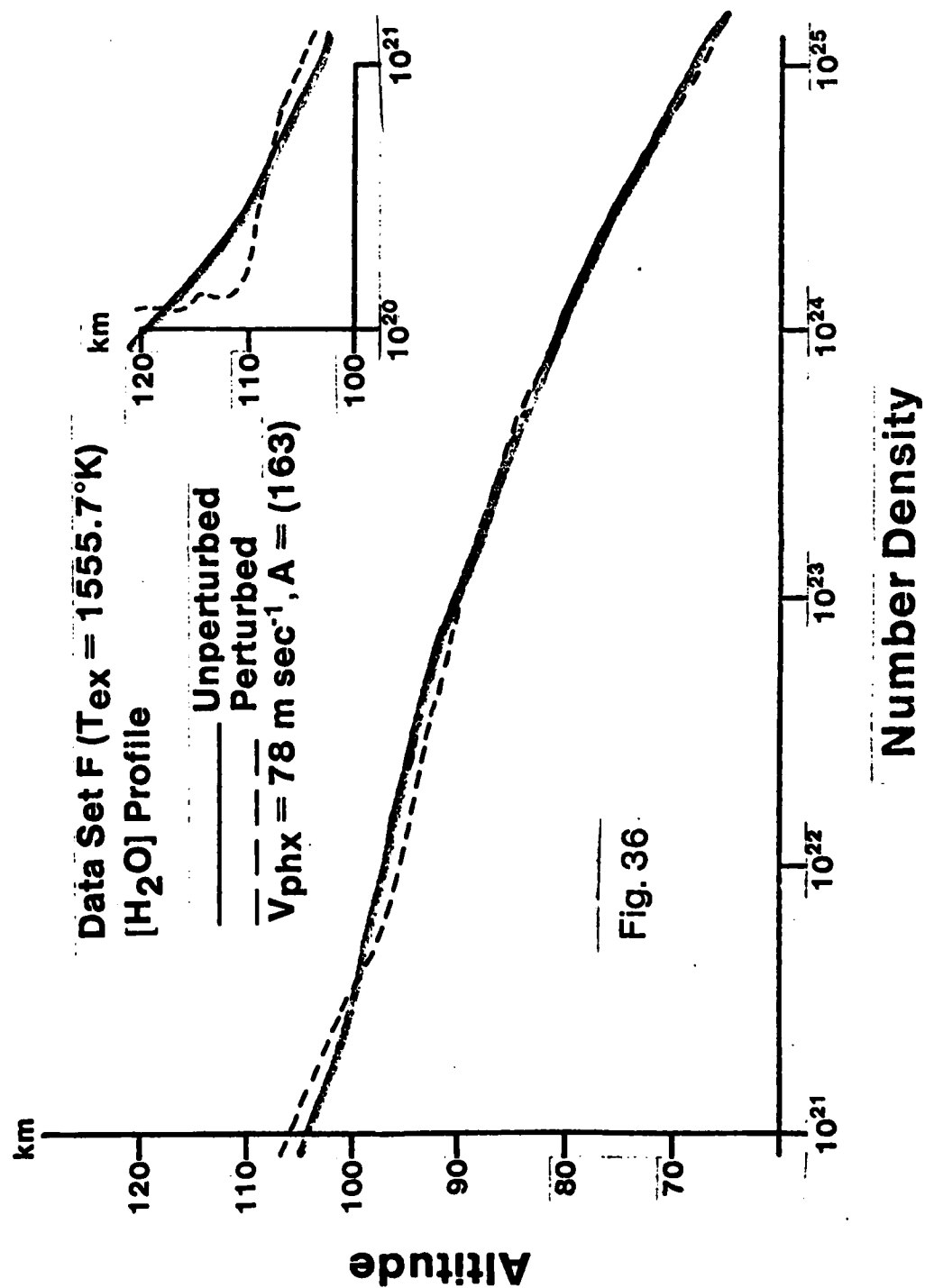--- Perturbed
V_{phx} =60 m sec^{-1}
(A=278)

Fig. 33

Number Density

Altitude

Data Set A (T_{ex} = 626.5°K)
[H_2O] Profile

—— Unperturbed
— — Perturbed
$\overline{V_{phx}}$ = 78 m sec⁻¹, A = (163)

Fig. 34

Number Density

Altitude

Data Set C (T_{ex} = 1081.2°K)
[H_2O] Profile

—— Unperturbed
— — — Perturbed
$\overline{V}_{phx}$ = 78 m sec^{-1}, A = (163)

Fig. 35

Number Density

Altitude

km^{-3}

km^{-3}

km

km

Data Set F ($T_{ex} = 1555.7°K$)
[H_2O] Profile

—— Unperturbed
— — Perturbed
$\overline{V}_{phx} = 78$ m sec^{-1}, A = (163)

Fig. 36

Number Density

Altitude

Data Set G ($T_{ex} = 1829.4°K$)
$[H_2O]$ Profile

—— Unperturbed
— — — Perturbed
$\overline{V}_{phx} = 78$ m sec^{-1}, A = (163)

Fig. 37

Number Density

Altitude

Data Set H ($T_{ex} = 2176.8°K$)
[H_2O] Profile

——— Unperturbed
— — — Perturbed
$\overline{V_{phx}} = 78$ m sec^{-1}, A = (163)

Fig. 38

Number Density

Altitude

Data Set A (T_{ex} = 626.5°K)
Day [NO] Radiance Profile, (Band center = 5.325 μm)
——— Unperturbed
– – – Perturbed
$\overline{V}_{phx}$ = 60 m sec^{-1}, A = (278)

Fig. 39

Infrared Radiance

Watts cm^{-3}

Altitude

km

120
110
100
90
80
70

-17
-18
-19

- 80 -

Data Set A ($T_{ex} = 626.5°K$)
Night [NO] Radiance Profile, (Band center = 5.325 μm)
—— Unperturbed
— — — Perturbed
$\overline{V_{phx}} = 60$ m sec^{-1}, A = (278)

Fig. 40

Infrared Radiance

Watts cm^{-3}

Altitude

km
120
110
100
90
80
70

-19
-18
-17

Data Set F (T_{ex} = 1555.7°K)
Day [NO] Radiance Profile, (Band center = 5.325 μm)
—— Unperturbed
– – – Perturbed
$\overline{V}_{phx}$ = 78 m sec^{-1}, A = (163)

Fig. 41

Infrared Radiance

Watts cm^{-3}

Altitude

Data Set F (T_{ex} = 1555.7°K)
Night [NO] Radiance Profile, (Band center = 5.325 μm)
——— Unperturbed
— — — Perturbed
$\overline{V}_{phx}$ = 60 m sec⁻¹, A = (278)

Fig. 42

Infrared Radiance

Watts cm⁻³

Altitude

km

Fig. 42

Data Set H (T_{ex} = 2176.8°K)
Day [NO] Radiance Profile, (Band center = 5.325 μm)
——— Unperturbed
— — — Perturbed
$\overline{V}_{phx}$ = 60 m sec^{-1}, A = (278)

Fig. 43

Infrared Radiance

Altitude

km

Watts cm^{-3}

- 84 -

Data Set H ($T_{ex} = 2176.8°K$)
Night [NO] Radiance Profile, (Band center = 5.325 μm)
—— Unperturbed
— — — Perturbed
$\overline{V_{phx}}$ = 60 m sec⁻¹, A = (278)

Fig. 44

Infrared Radiance

Altitude

km

120
110
100
90
80
70

-18
-17
-16
-15

Watts cm⁻³

Fig. 45

$T_{ex} = 1500^{\circ}K$

——— WINTER

Period = 7.5 min.

POTENTIAL $\frac{KM2}{SEC2}$

ALTITUDE (km)

Fig. 46

T_A=acoustic frequency cut-off
T_B=Brunt period

Altitude in KM

Period in Minutes

Fig. 47

- 88 -

Zenith referred all-sky map at 1.65μ
obtained the evening of 2 December 1972
at Capilla Observatory.
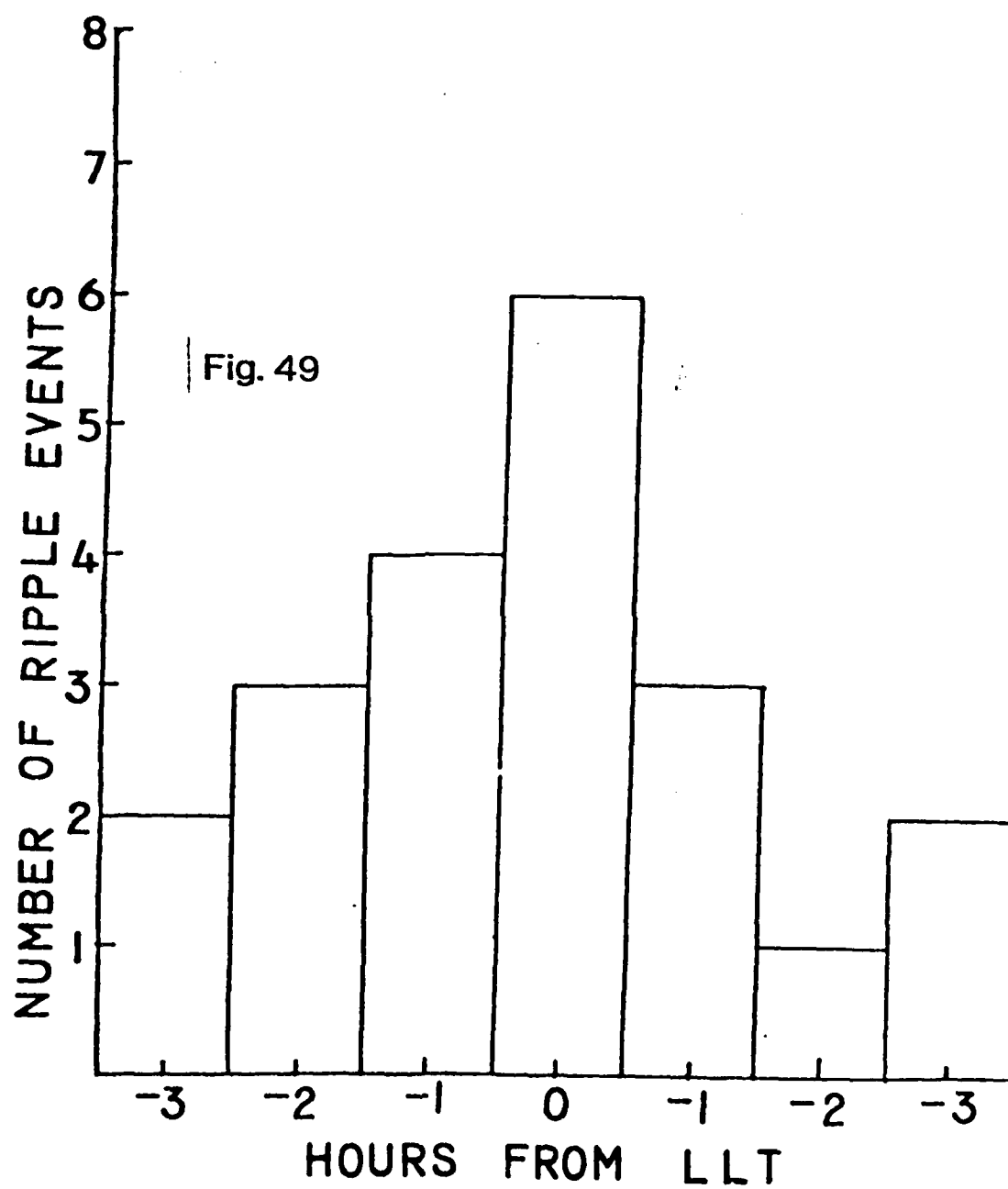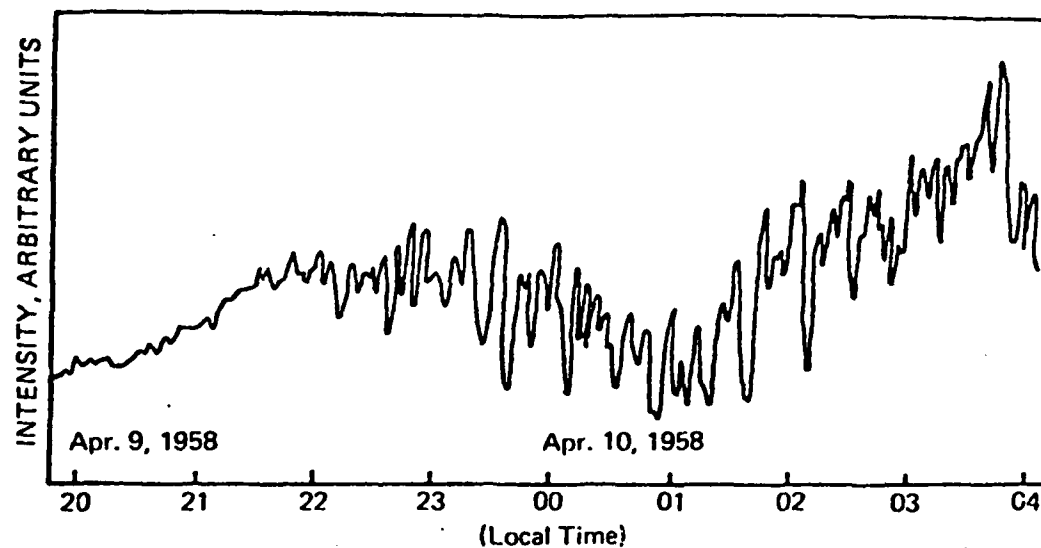
Fig. 49
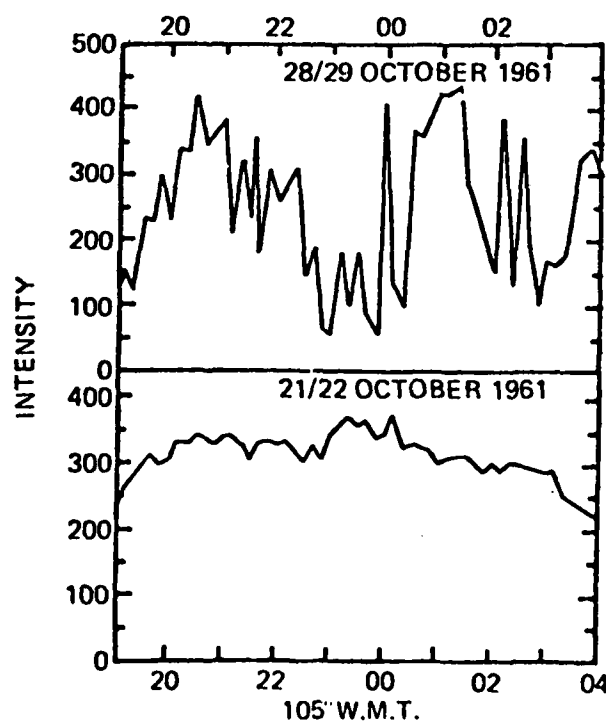
Apr. 9, 1958   Apr. 10, 1958

(Local Time)

Fig. 50
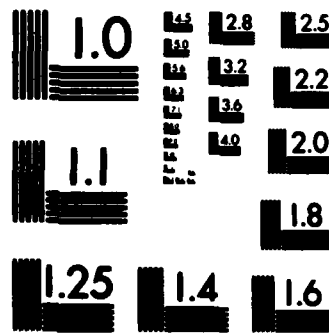

28/29 OCTOBER 1961

21/22 OCTOBER 1961

105° W.M.T.

Fig. 51

END

FILMED

DTIC

MICROCOPY RESOLUTION TEST CHART

NATIONAL BUREAU OF STANDARDS-1963-A

Fig. 52

Period = 1 hour X_0 = 1.58 km k_z = .628 km^{-1}

Local Time in Hours

Altitude in km

1 hr.   2 hrs.   3 hrs.   4 hrs.

$x^0 = 1.702$ KM
$T = 2.0$ hours

Turbulence

$Ri \geq \frac{1}{2}$

Turbulence

$Ri \geq \frac{1}{2}$

Turbulence
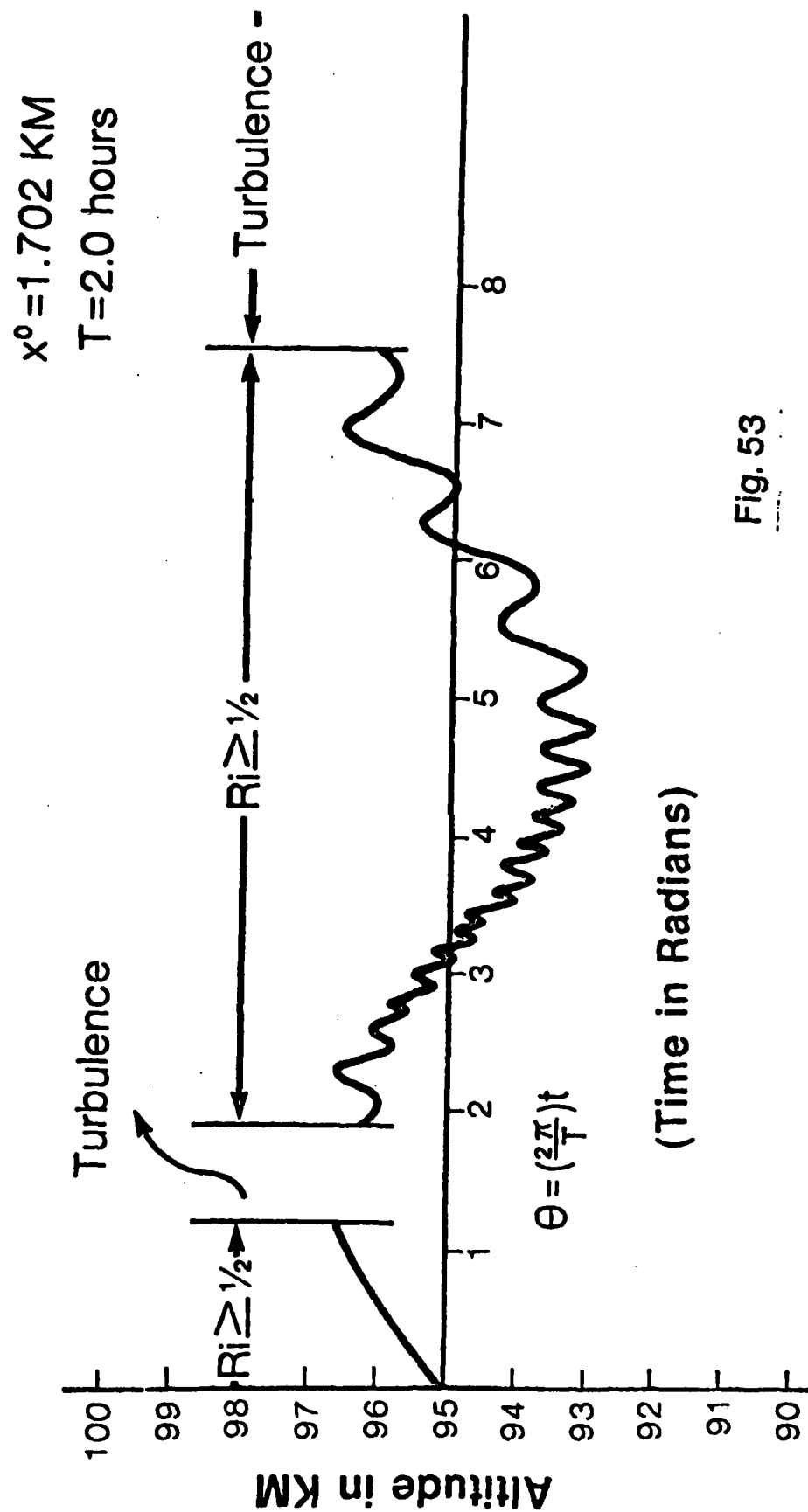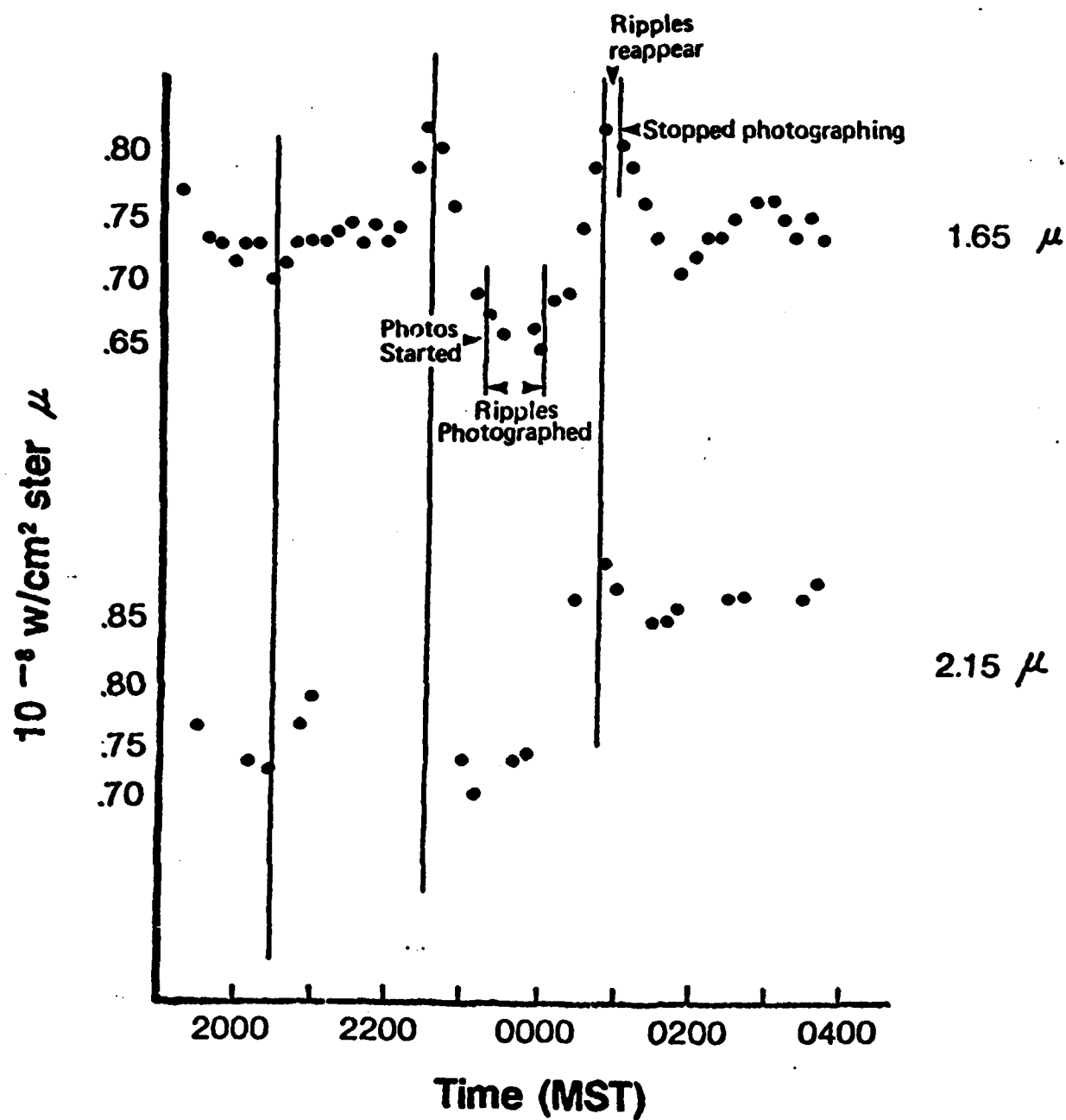
$\theta = (\frac{2\pi}{T})t$

(Time in Radians)

Altitude in KM
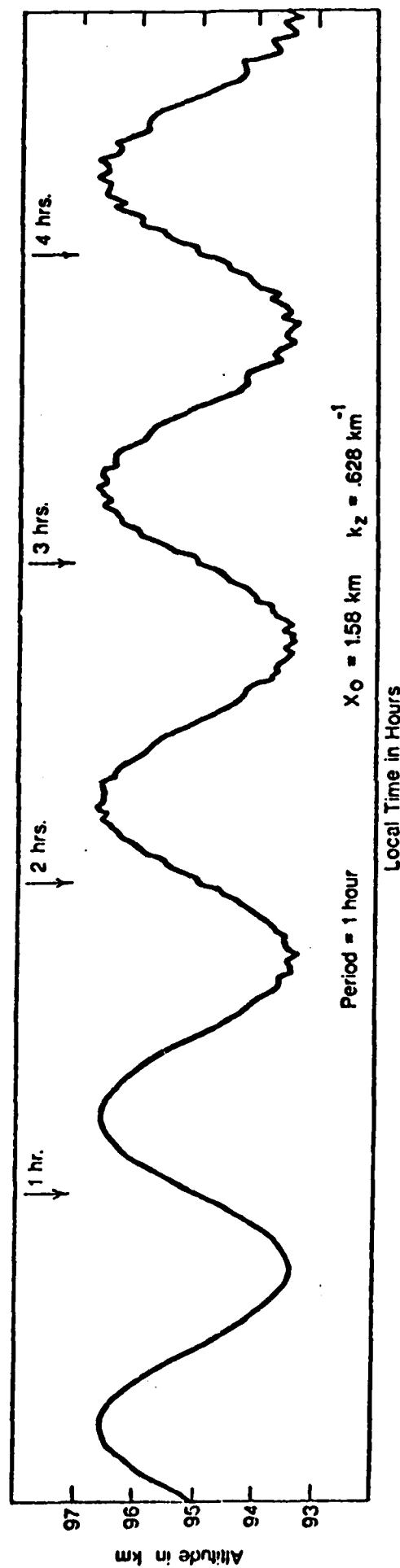
Fig. 53

Fig. 54

2—3 Feb 1973

END

FILMED

12-84

DTIC